

Part consolidation for additive manufacturing: a multi-layered topology optimization approach

Luke Crispo, Il Yong Kim

Department of Mechanical and Materials Engineering, Queen's University Kingston, Canada

Correspondence

Il Yong Kim, Department of Mechanical and Materials Engineering, Queen's University, Kingston, ON, K7L 3N6, Canada
Email: kimiy@queensu.ca

Summary

Part consolidation is becoming a viable cost savings approach due to the increased design freedom associated with industry adoption of additive manufacturing. However, there is little research focused on mathematical approaches for assembly-level design generation, with most work aimed at providing best practices for merging several parts into one. This paper presents a novel topology optimization approach to part consolidation that determines the ideal number of parts, their geometry, and optimal joining pattern, without bias towards the original assembly. Multiple layered design domains are created, and a joining domain that determines the connections between parts is introduced. A multi-objective problem statement optimizes the complex trade-off between compliance, support structure volume, surface area, and number of joints, to minimize the total cost of the final assembly. Design variable initialization and boundary condition placement are discussed for problems with multiple domains. Three test cases are presented and solved for a range of cost trade-offs to demonstrate optimized solutions as design objectives are varied.

Keywords: part consolidation, design for additive manufacturing, multicomponent topology optimization, multi-layered approach

1 INTRODUCTION

Additive Manufacturing (AM) is a rapidly growing technology that allows for the fabrication of complex designs by building a part one layer at a time as opposed to the traditional subtractive or formative techniques. The added geometric complexity enabled by AM can generate features that are cost-prohibitive or in some cases impossible to produce with traditional manufacturing methods. This increased design freedom can improve performance and decrease cost if parts are redesigned for the AM process. Recent advancements in metal additive manufacturing [1, 2] have increased the feasibility of using AM in the aerospace industry, where low volumes and high-performance requirements allow for design exploration in the latest technologies.

Topology Optimization (TO) is a computational tool that generates an ideal material distribution to maximize the performance of a design subject to specified constraints. Since its conception by Bendsoe and Kikuchi [3], there has been widespread research in TO with Deaton and Grandhi summarizing recent developments [4] and Sigmund and Maute providing a comparative review of the different topology optimization approaches [5]. There has also been extensive application of topology optimization in industry realizing improved performance and reduced cost. Wong, Ryan, and Kim applied topology optimization under dynamic loading to reduce weight and cost of an aircraft landing gear assembly [6], while Li, Kim, and Jeswiet used topology, shape, and size optimization to decrease the weight of an automotive engine cradle subject to stiffness and natural frequency constraints [7]. While gradient-based optimization techniques are most often used in TO, black box topology optimization approaches may become an effective alternative for solving multi-objective, nonlinear optimization problems [8].

Additive manufacturing is an ideal candidate for fabricating topology-optimized designs as the resulting complex geometry can be printed with minimal interpretation, eliminating the associated reduction in performance. There has therefore been significant research focused on integrating topology optimization algorithms with the AM driving factors for cost and performance, known as design for additive manufacturing [9, 10]. These methodologies generally focus on the penalization or minimization of support structure volume, which increases material cost and print time, or the reduction of small features that may fail during printing. Mhapsekar et al. introduced a layer-based density filter that penalized small features, calculated support structure requirements based on the layer of elements below the element of interest, and minimized support structure volume using a multi-objective approach [11]. Langelaar presented a methodology for optimizing part geometry while simultaneously minimizing the support structure of N discrete printing orientations with an AM filter identifying support volume requirements. This technique gradually narrows its focus and selects an ideal printing orientation for the optimized geometry [12]. Ryan and Kim leveraged density gradients to identify exterior surfaces and directly calculate support structure volume. Compliance, surface area, and support structure volume were minimized through multi-objective topology optimization [13]. Sabiston and Kim improved the practicality of this methodology through a 3D implementation and verified its capability by printing several test problems resulting in a 29-38% reduction in print time and a 45-76% reduction in support volume requirements [14]. Support structures themselves have also been topology optimized by Mezzadri et al. to reduce mass and ensure adequate stiffness and support for the printed geometry [15]. Another area of interest bridging AM and TO is the optimization of component infill which Schmitt, Mehta, and Kim concluded has a significant impact on the material properties of a component [16].

Part Consolidation (PC) is a design technique enabled by AM where several parts previously assembled together are printed as a single piece. This can significantly reduce assembly labor time, supply chain requirements, and lead time, ultimately reducing the associated costs by up to 85% in select case studies [17]. The combination of PC and AM can also improve design performance as showcased by Schmelzle et al. during the redesign of a hydraulic manifold, resulting in a 60% decrease in weight while improving performance and reducing failure points [18]. While it may seem ideal to consolidate every assembly into a single part, there are often factors that prevent the

part from being manufactured in a single piece as outlined in Figure 1. Build plate size constraints limit the maximum dimensions of a part that can be printed and are relevant because large AM machines may be cost prohibitive. Internal voids are impossible to manufacture without leaving unnecessary support structure or unmelted metal powder inside the cavities. There are also a wide range of functional requirements that can prevent consolidation in a single piece, such as relative motion, assembly considerations, standardized electronic components, or disassembly for maintenance as outlined by Yang and Zhao [19].

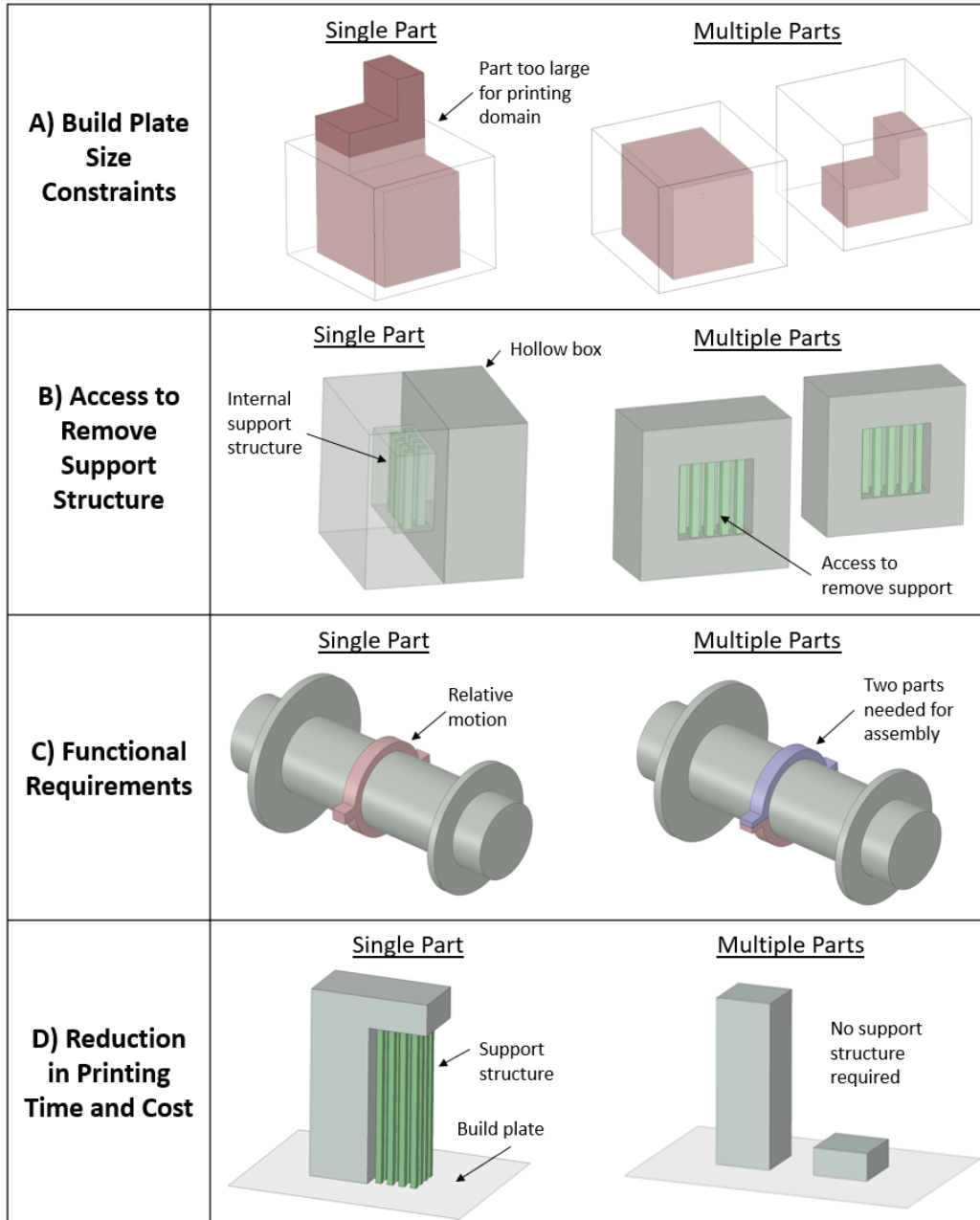


Figure 1: Overview of factors preventing consolidation into a single part accompanied by simplified examples. Note that C) presents relative motion and assembly considerations as examples of functional requirements and D) assumes that the printing orientation is fixed.

The overall cost of a design is a consideration that may discourage consolidation into a single part, compared to the previously discussed criteria which strictly prevent printing in a single piece. Knofius et al. concluded that as more parts are consolidated, the resultant parts become more complex, reducing the possibility that the consolidation is beneficial when considering a logistics, manufacturing, and repair perspective [20]. A review of assembly-based design for additive manufacturing concluded that part decomposition (splitting a single part into multiple parts) can improve AM printability, process time, material costs, and overall quality [21]. In a different study, Oh et al. outlined a direct trade-off between build time and assembly time as the number of parts in an assembly changes, and identified the existence of an optimal number of parts that reduces overall processing time [22]. Guirguis et al. considered a similar trade-off between manufacturing cost and assembly cost in a multi-objective problem statement to minimize the overall cost of sheet metal and composite assemblies [23, 24]. This work presented a pareto frontier of assembly cost and manufacturing cost that demonstrated a direct trade-off between the cost objectives that must be considered to reduce overall cost. Figure 1D) shows a simplified example of the trade-off between support volume costs and assembly costs assuming the printing orientation of the part is fixed. The single part has no assembly time but a long printing and post processing time while the assembly has a faster printing time that requires minimal post processing but has a longer assembly time. This trade-off can result in a multi-component design with a lower overall cost than a single part design depending on the ratio of printing and assembly costs.

A part consolidation problem can be considered from either a top-down approach that uses the baseline assembly as a starting point, or a bottom-up approach that starts from the design space in the problem definition. Figure 2 outlines three levels of part consolidation with examples from a hypothetical baseline geometry and design space, where Levels 1 and 2 show a top-down approach and Level 3 outlines a bottom-up approach. The problem statement outlines the available design and non-design space of the problem along with the structural loading. The baseline geometry shows a sample assembly manufactured with traditional subtractive techniques that is the subject of the part consolidation problem. Level 1 PC starts from the original assembly design and combines individual parts together. This reduces both the number of parts and joints, but severely limits the design freedom of the resulting geometry as it is still limited by the manufacturing constraints of the original assembly. Level 2 PC involves first completing Level 1 consolidation followed by a redesign or optimization of each resulting part. While improving the design freedom from Level 1, the redesign is completed after the part combination and alternate connections between parts are not considered. A study by Liu concluded that simultaneously optimizing factors such as structural performance, build direction, and joint positions can improve the performance of a consolidated part [25]. These concerns are addressed by Level 3 PC which splits the baseline design space into parts, simultaneously designing the part and joint geometry. This allows for an unlimited number of part combinations and can result in assembly designs that are not possible to create with top-down approaches.

Research in PC has developed a collection of guidelines and recommendations for best practices along with several PC case studies. Rodrigue and Rivette performed Level 2 PC by considering relative motion and assembly/disassembly requirements and redesigning the resultant structural design space through topology optimization [26]. Yang et al. [27] and Soussou et al. [28]

independently proposed Level 2 PC methods where parts are consolidated by determining the functional interfaces of an assembly, generating functional volumes that link functional surfaces together, and performing structural optimization on the functional volumes. The hydraulic manifold PC case study by Schmelzle et al. applied Level 2 PC to an industry problem using a manual redesign process [18]. Reiher et al. consolidated parts that shared a single function (such as a bracket assembly) and conducted Level 2 PC by applying TO on the combined geometry [29]. Yang et al. developed a numerical algorithm that automatically identifies candidates for Level 1 PC by considering a variety of functional criteria that prevent consolidation [30].

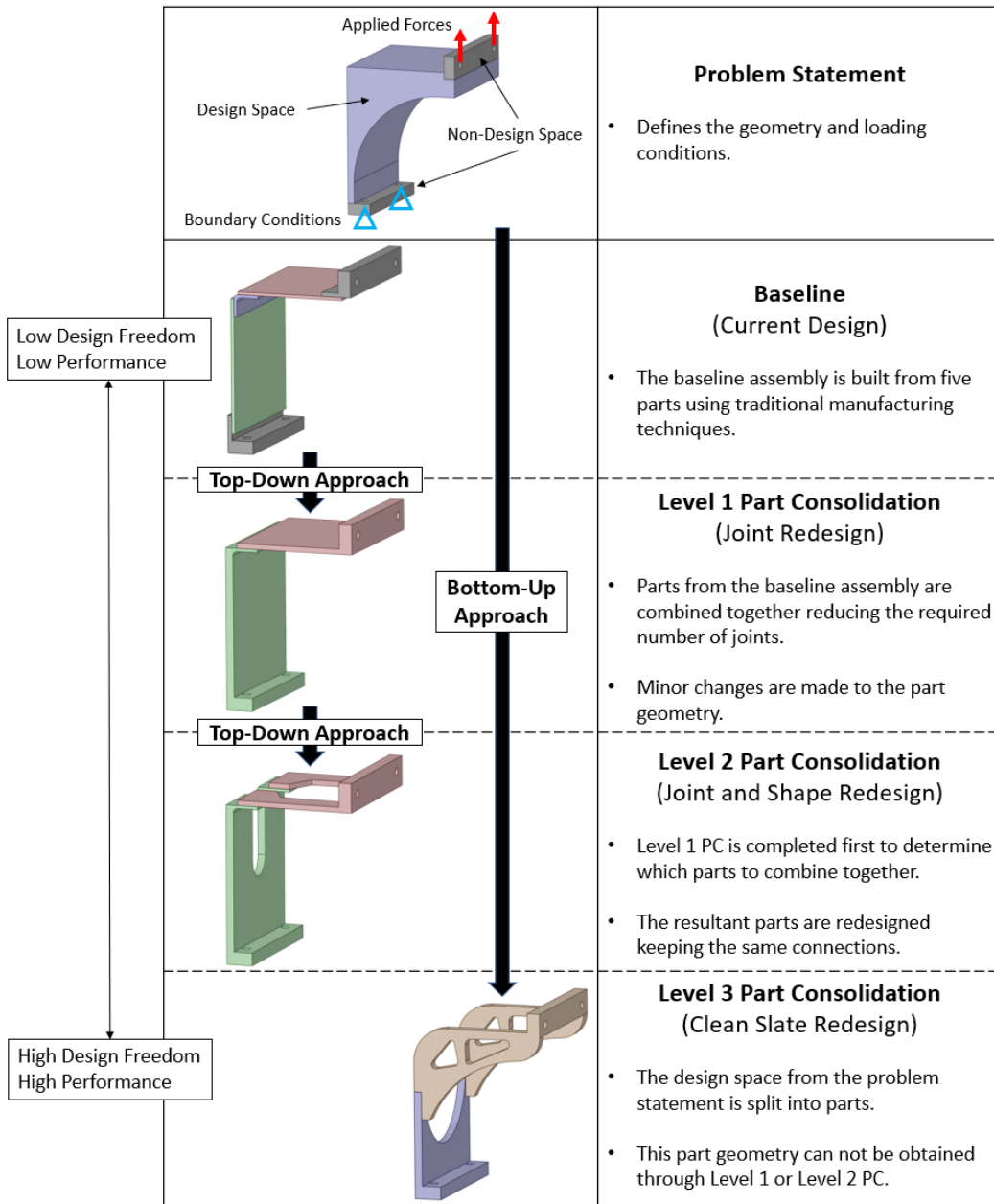


Figure 2: Summary of the different levels of part consolidation applied to a hypothetical problem statement and baseline assembly design. Levels 1 and 2 represent a top-down approach that limits design freedom, while Level 3 outlines a bottom-up approach that can result in an unlimited number of part combinations.

To integrate part consolidation with topology optimization, as shown in Level 3 in Figure 2, a new TO approach must be developed for the design of an assembly instead of an individual part. Chickermane and Gea presented an assembly topology optimization approach with multiple part regions and a preselected interconnection region that dictated the general structure of the final design [31]. Connections were modelled using spring elements with a stiffness controlled by design variables and a constraint placed on the maximum number of permissible connections. Li et al. determined optimal joint placement between two fixed parts using an evolutionary structural optimization method to eliminate joints based on their structural efficiency [32]. Zhu et al. developed an approach that simultaneously optimized structural topology and found the ideal layout of moveable components with fixed geometry within the TO domain [33]. Swartz and James proposed a topology optimization approach for the design of multi-body compliant mechanisms that defined part geometry through multiple overlapping layers and used link elements to connect between layers [34]. The number of connections was defined in advance and the x-y location of connections was optimized while updating the stiffness of link elements through a Gaussian stiffness distribution to model a pinned joint. Guirguis et al. presented a level set methodology for multi-component topology optimization of sheet metal assemblies [23, 24]. Connections between parts were modelled using a custom finite element mesh and overall cost was minimized in both a two stage and single stage approach.

Recent publications by Zhou et al. proposed a multi-component topology optimization algorithm that optimizes overall assembly geometry through a density field and splits the design space into parts through the definition of component membership design variables [35, 36]. This method performs Level 3 assembly design but is not aimed towards part consolidation because the problem statement, minimizing compliance subject to feasibility constraints (including internal void removal and build plate volume restrictions), does not consider costs (such as support structure volume or assembly costs). All interfaces between parts are assumed to be joined and connections between parts are artificially weakened due to the regularization scheme applied to the component membership field. The placement of joints along the interface is not explicitly designed by this formulation. Crispo and Kim proposed an assembly level topology optimization approach that models multiple components using overlapping part domains and a joining domain to determine the existence of connections between parts [37]. This methodology explicitly determined part and joint geometry using Level 3 part consolidation, but division of design space into parts was influenced solely by the problem initialization as additive manufacturing costs were not considered.

Assembly level topology optimization is indirectly considered in multi-material topology optimization (MMTO) where both part layout and material use are optimized to generate lightweight designs with improved performance over a single material part [38]. Woischwill and Kim formulated a novel multi-material and multi-joint topology optimization algorithm that models joints using a custom finite element mesh to account for the reduction in stiffness that occurs at the interface between materials, and optimized the connection pattern accordingly [39]. This approach was expanded by Florea et al for 3D problems and the addition of tooling accessibility constraints to ensure connections were feasible to manufacture [40].

1.1 Knowledge Gap

No computational methods exist in literature that perform bottom-up part consolidation considering both assembly and additive manufacturing part costs. The majority of part consolidation literature manually performs top-down part consolidation, with the only bottom-up computational approach neglecting assembly costs.

The top-down approach restricts the design freedom of the final consolidated assembly as there is only a finite number of part combinations. This restriction, which can be considered a constraint from an optimization perspective, may result in a sub-optimal design. A bottom-up approach that actively divides the overall design space into parts instead has an unlimited number of assembly combinations and may result in consolidated designs with improved performance.

All PC research in AM assumes that reducing the number of parts in an assembly will reduce the overall cost and that therefore minimizing the number of parts under given design constraints will in turn minimize the cost of the assembly. However, there are a variety of factors that influence the overall cost of an AM assembly, such as printing time and support structure removal costs, both of which typically increase as more parts are consolidated. There is a complex mechanism relating the reduction in cost from removing joints or parts (less assembly and handling time) and the increase in cost that occurs from combining multiple parts together (increased part complexity results in longer print and post processing time). Without modelling this mechanism, the trade-off between these costs can not be assessed. There are no PC studies in literature that consider this trade-off and therefore previous PC approaches are not formulated to reduce the overall cost of an AM assembly.

Previously proposed density-based multi-component TO approaches are not well suited for part consolidation problems as they either predefine some portions of the geometry, do not determine the ideal joining connection between parts, or are not formulated in a way that allows for easy identification of individual components.

1.2 Objectives

The objective of this paper is to develop a new topology optimization methodology for part consolidation that can consider assembly cost, in addition to AM part cost, based on a bottom up approach. The proposed method accomplishes this objective by:

1. Minimizing the total cost of an assembly by considering the complex mechanism relating both joining cost and individual part cost.
2. Following a bottom-up approach that improves design freedom by starting from a clean slate design space.
3. Simultaneously determining the optimal part geometry, number of parts to consolidate, and ideal connection layout of an assembly.

2 PROBLEM FORMULATION

In order to approach part consolidation from a topology optimization perspective, the traditional topology optimization domain and design variables must be modified to account for the geometry

and joining of multiple parts. A new methodology is proposed that is developed specifically for the part consolidation problem outlined in this paper.

The foundation of the proposed methodology for modelling connections is based on the following principles:

1. Connections transfer loads between parts in specified degrees of freedom (depending on the connection type). Loads cannot be transferred between two unconnected parts.
2. The stiffness of the connection is different from the stiffness of the material. The stiffness of the connection (or of the surrounding area for a weld) is typically lower than that of the material.

The proposed methodology is focused on the design of static structural assemblies and therefore all degrees of freedom are connected at joint locations. The type of connection (adhesive, bolt, weld) is not specified as this typically depends on the industry application and any associated joining requirements. Therefore, no attempt is made to model the complex structural mechanics of a particular connection type. Instead, the goal is to consider the difference in stiffness that occurs at connections throughout the topology optimization process. For the remainder of this paper, the terminology “joint” refers to a generic connection and it is assumed that any connections between parts in the optimized design will be refined after the optimization according to the appropriate industry requirements.

2.1 Multi-Layered Topology Optimization

The optimization problem statement presented in (1) is formulated to accomplish the proposed objectives by minimizing the weighted sum of structural compliance, C , number of joints in the assembly, Γ , total support structure volume, Λ , and total surface area of the parts, Φ . The weighting factors represent a series of relative trade-offs between two objectives, where w_1 is the weighting between structural compliance and overall cost, w_2 is the weighting between joint cost and part cost, and w_3 is the weighting between support structure cost and surface area cost. A weighting factor of $w_i = 1$ indicates a full weighting given to the first objective, while $w_i = 0$ indicates a full weighting given to the second objective. C_0 , Γ_0 , Λ_0 , and Φ_0 normalize the respective objective functions to ensure similar magnitudes in the multi-objective approach. The design variable \underline{x} represents a column vector of element densities that determines the topology of each part in the assembly, while \underline{y} is the column vector of nodal joint densities that identifies the existence of joints.

$$\begin{aligned}
 \text{minimize : } J = & w_1 \frac{C(x, \underline{y})}{C_0} + (1-w_1) \left(w_2 \frac{\Gamma(\underline{y})}{\Gamma_0} + (1-w_2) \left(w_3 \frac{\Lambda(\underline{x})}{\Lambda_0} + (1-w_3) \frac{\Phi(\underline{x})}{\Phi_0} \right) \right) \\
 \text{subject to : } & \underline{K}\underline{u} = \underline{f} \\
 & \sum_{e=1}^N x_e V_e \leq \gamma V_0 \\
 & 0 \leq x_e \leq 1 \quad \forall e \in \Omega \\
 & 0 \leq y_j \leq 1 \quad \forall j \in \Omega \\
 & 0 \leq w_i \leq 1 \quad i=1,2,3
 \end{aligned} \tag{1}$$

The optimization is subjected to a structural, linear static governing equation constraint where \underline{K} is the global stiffness matrix of the assembly, \underline{u} is the vector of nodal displacements, and \underline{f} represents the vector of applied forces. A volume fraction constraint is enforced where x_e is the density of the e th element (with N total elements), V_e is the element volume, γ is the specified volume fraction, and V_0 is the total volume of the design space. Element densities, x_e , are restricted between zero representing a void and unity representing material existence. The nodal joint density, y_j , of the j th joint also vary continuously where $y_j = 0$ represents no connection and $y_j = 1$ indicates the presence of a joint. Finally, each specified weighting factor must fall within the desired range.

This paper proposes the Multi-Layered Topology Optimization (MLTO) approach to model multiple parts with L identical, overlapping, but disconnected part domains. The finite element mesh of each layered part domain is identical and built from the original assembly design space. Each part domain is discretized into n elements and the assembly geometry is specified by a column vector of element densities \underline{x} with a length of $N = n * L$. The separation of parts into individual domains is crucial to this formulation and separates this technique from other approaches (such as MMTTO where a design variable vector determines the material or part for each element) as it allows for the calculation of support structure volume, identification of build plate height, and selection of the ideal print direction uniquely for each part domain.

The L layered part domains are supplemented by a single joining domain that identifies the existence of joints at each node of the original design domain specified in the design variable \underline{y} with a length of M . Figure 3 (A) demonstrates the overlapping MLTO domains in an expanded view. Figure 3 (B) outlines a sample assembly design on an individual domain level while Figure 3 (C) shows the overlapping assembly design. While this figure outlines a 2D geometry with individual domains represented by 2D planes, this concept is also applicable in three dimensions where the 3D assembly geometry would be represented by domains that are overlapping 3D volumes.

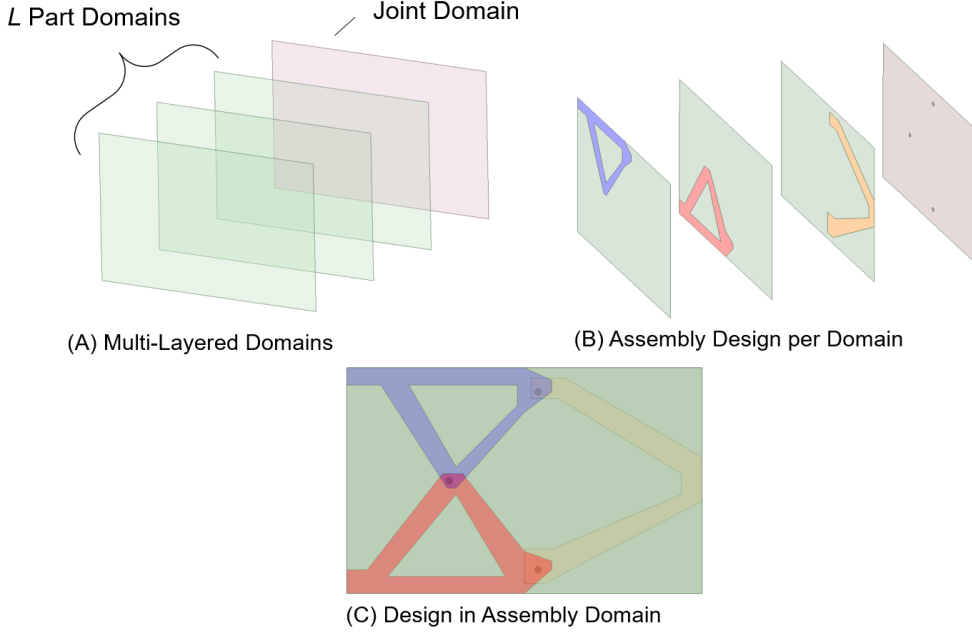


Figure 3: Outline of the MLTO approach for assembly level topology optimization where (A) outlines the L part domains and single joining domain. Note that domains are separated for conceptualization. (B) shows a sample assembly design represented on an individual domain level with (C) representing the combined design as an assembly.

The elastic modulus of each element is interpolated using a modified Solid Isotropic Material with Penalisation (SIMP) method [41]

$$E_e = E_e(x_e) = E_{\min} + x_e^p (E_0^1 - E_{\min}), \quad (2)$$

where E_e is the penalized Young's Modulus of the e th element, E_{\min} is an arbitrary small non-zero number representing the stiffness of void material, p is the element penalty factor, and E_0^1 is the material elastic modulus.

A joint is modelled structurally by a set of linear bar elements connecting the appropriate degrees of freedom between part domains. In a problem without rotational degrees of freedom (i.e. no beam or shell elements), a single bar element per spatial dimension is required to connect two domains. The stiffness of each bar element is defined similar to element stiffness as

$$E_j = E_j(y_j) = E_{\min} + y_j^q (E_0^2 - E_{\min}), \quad (3)$$

where E_j is the interpolated stiffness of the j th joint, q represents the joint penalty factor, and E_0^2 is the base joint stiffness. The stiffness matrix of a bar element is modified from the standard formulation

$$[\tilde{K}^{\text{bar}}] = \frac{AE}{l} \begin{bmatrix} 1 & -1 \\ -1 & 1 \end{bmatrix}, \quad (4)$$

by replacing the area A , Young's Modulus E , and length l , with the interpolated joint stiffness $E_j(y_j)$ resulting in

$$[\tilde{K}^{\text{mod}}] = E_j(y_j) \begin{bmatrix} 1 & -1 \\ -1 & 1 \end{bmatrix}, \quad (5)$$

where \tilde{K}^{mod} is the modified bar stiffness matrix connecting a single degree of freedom between domains. This substitution indicates that E_0^2 is not a material elastic modulus and therefore cannot be directly compared to the Young's Modulus of the material or of the joint. It is instead defined as the stiffness of a fully solid joint with units of [Force/length] and is conceptually equivalent to a spring constant. The base joint stiffness can be approximated using empirical calculations such as those outlined in the Douglas or Huth fastener models [42]. These empirical models are not directly applicable to the problem formulation presented in this methodology and may need to be adjusted to obtain more meaningful results during optimization. A bar element was used in this formulation; however, a similar derivation could be conducted for a beam element if the finite element model requires the restriction of rotational degrees of freedom. In finite element formulations where joint stiffness is dependent on how the joint is loaded (such as in axial, shear, or torsion) it is recommended to use average directional joint stiffness properties during optimization and to refine the joint model when interpreting optimization results.

The stiffness matrix of a joint connecting two domains can be represented as the sum of the modified bar element matrices of each spatial dimension, represented as

$$\tilde{K}_c^{\text{sub-joint}} = \sum_k^{N_d} \tilde{K}_k^{\text{mod}} = E_j(y_j) \tilde{K}_c^0, \quad [\tilde{K}_c^0] = \begin{bmatrix} I & \cdots & -I \\ \vdots & \ddots & \vdots \\ -I & \cdots & I \end{bmatrix}, \quad (6)$$

where $\tilde{K}_c^{\text{sub-joint}}$ is the stiffness matrix of the sub-joint of the c th connection, \tilde{K}_k^{mod} represents the modified stiffness matrix of the k th dimension (N^d total dimensions), and I is the identity matrix of dimension equal to the number of spatial dimensions. \tilde{K}_c^0 is the generalized sub-joint stiffness matrix of the c th connection with entries equal to 1 for degrees of freedom that are connected and zero for those that are unconnected. Each c th sub-joint connection joins all degrees of freedom between only two domains. Therefore, only one sub-joint is required per node when two domains are used ($L = 2$).

When there are more than two overlapping part domains ($L > 2$), additional sub-joints must be placed per node to connect to all domains. The placement of these sub-joints between domains has a significant impact on the overall stiffness of the joint. The following criteria are used to identify a combination of sub-joint connections that represents a real-world joint and allows for smooth convergence of the design without a bias towards any domain:

1. Joints should connect between all part domains at every node, even if there is no density at a specific location. This allows for emerging density to develop in a new domain, as

increasing an unconnected element's density would not change the compliance of the assembly.

2. There should never be more than one load path between two domains at a single node, as this would strengthen that connection. In other words, no two design domains should be connected by more than one sub-joint.
3. A load path between two domains should never pass through an intermediate domain if the intermediate node is surrounded by empty elements. If this occurs, it means that two bar elements are chained together in series, artificially reducing the stiffness of the connection.

The combination of the first and second principle indicate that exactly $L-1$ sub-joints should be placed per node, while the third principle is instead related to how the sub-joints should be placed between domains. All criteria are satisfied if sub-joints are placed from the part domain with maximum element density at that location (surrounding the node) to all other part domains. Starting each connection at a node from the same domain ensures that there will be only one load path between domains. The selection of the domain with the largest element density ensures that no connection passes through a domain with empty element density. This connection pattern can be expressed as

$$[\underline{G}_j] = \begin{bmatrix} d_j^{\max} & d(i=1) \\ \vdots & \vdots \\ d_j^{\max} & d(i=L) \end{bmatrix} \quad \text{where } d(i) = \begin{cases} i, & i \neq d_j^{\max} \\ 0, & i = d_j^{\max} \end{cases}, \quad (7)$$

where \underline{G}_j is the matrix of connections for the j th node, d_j^{\max} represents the part domain with maximum element density around the j th node, and $d(i)$ represents the second part domain being connected by that sub-joint. Each row of \underline{G}_j represents a connection between the domains specified in columns one and two. The row with a value of zero in the second column is neglected as it represents no connection (where the domain with maximum density would be connecting to itself).

The total stiffness matrix of a joint at one node including all bar elements for all connections between domains as defined in (7) is calculated as the sum of all sub-joints

$$\underline{K}_j = \sum_{c=1}^{L-1} \underline{K}_c^{\text{sub-joint}} = E_j(y_j) \sum_{c=1}^{L-1} \underline{K}_c^0, \quad (8)$$

where \underline{K}_j represents the joint level stiffness matrix. The global stiffness matrix of the assembly, \underline{K} , is calculated as the sum of all element and joint stiffness matrices or can also be represented on a domain level stiffness as

$$\underline{K} = \sum_{e=1}^N E_e(x_e) \underline{K}_e^0 + \sum_{j=1}^M \left(E_j(y_j) \sum_{c=1}^{L-1} \underline{K}_c^0 \right) = \sum_{d=1}^L \underline{K}_d + \sum_{j=1}^M \underline{K}_j, \quad (9)$$

where K_e^0 is the element level stiffness matrix and K_d represents the stiffness of the d th domain. Note that each part domain is completed uncoupled and contains unique degrees of freedom, while the joints connect the degrees of freedom between domains.

The compliance of the assembly can be calculated by the sum of the compliance of all individual elements within every part and joining domain as

$$C(\underline{x}, \underline{y}) = \sum_e^N (E_{\min} + x_e^p (E_0^1 - E_{\min})) \underline{u}_e^T K_e^0 \underline{u}_e + \sum_j^M (E_{\min} + y_j^q (E_0^2 - E_{\min})) \left(\sum_{c=1}^{L-1} \underline{u}_c^T K_c^0 \underline{u}_c \right)_j, \quad (10)$$

where \underline{u}_e represents the displacement vector of nodes associated with the nodes of element e , and \underline{u}_c is the displacement vector of all nodes associated with the sub-joint connection c of joint j identified by the connection pattern defined in (7).

2.2 Cost Modelling

To formulate a problem statement minimizing the cost of an assembly, the major cost-driving factors of an assembly must be identified. Then, a methodology must be developed to determine a mathematical representation of these cost-driving factors at any topology optimization iteration with intermediate density elements. The overall cost of an assembly can be split into part costs and joint costs as represented in Figure 4.

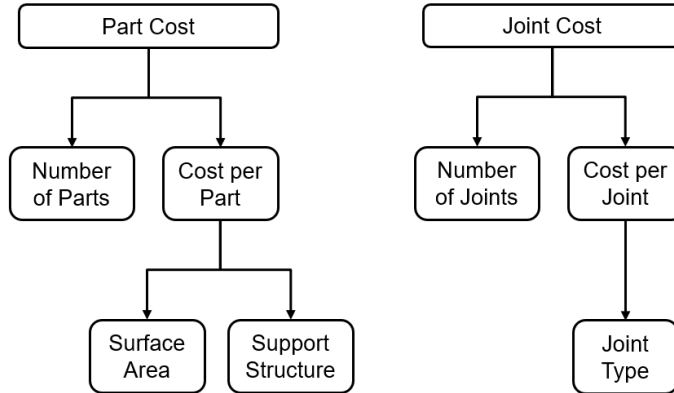


Figure 4: Summary of cost driving factors for an additive manufacturing assembly where cost-driving factors are grouped into part or joint costs.

The part cost is related to both the total number of parts and the cost per part but can be more accurately represented as the sum of each individual part cost. When considering the AM cost-driving factors as presented by Ryan and Kim [13], part cost can be represented as the weighted sum of surface area, Φ , and support structure volume, Λ , for all parts in the assembly. The core mathematical derivation of the cost driving factors for additive manufacturing of a single part are outlined by Ryan et Kim [13]. The derivation of these cost driving factors are presented below for the MLTO approach.

The Helmholtz density filter [43, 44] is implemented instead of traditional filtering approaches [41, 45, 46] as it is an efficient method for calculating the spatial gradient, which is crucial to the

calculation of surface area and support volume structure. The Helmholtz partial differential equation is given as

$$-r_H^2 \nabla^2 \tilde{\rho} + \tilde{\rho} = \tilde{x}, \quad (11)$$

where r_H is the length scale parameter analogous to the filter radius of sensitivity filters, $\tilde{\rho}$ is the vector of filtered element densities in a single domain, and \tilde{x} is the vector of unfiltered design variables in a single part domain. The Helmholtz equation is solved independently for each part domain as element densities should only be filtered based on other elements belonging to the same part. No filtering is applied to the joining domain as discrete joint locations are preferred. The spatial gradient of element density is then calculated as

$$\nabla \rho_e = \sum_{k=1}^{N_d} \tilde{B}_e^k \tilde{\rho} \hat{e}_k, \quad (12)$$

where $\nabla \rho_e$ is the spatial density gradient of the e th element, N_d is the number of spatial dimensions, \tilde{B}_e^k is the derivative of the e th element shape function in terms of the k th dimension, $\tilde{\rho}$ represents the vector of nodal filtered densities of one part domain, and \hat{e}_k is the basis vector of the associated spatial dimension. The surface condition number can be defined as

$$\Phi_e = \|\nabla \rho_e\| = \sqrt{\sum_{k=1}^{N_d} (\nabla_k \rho_e)^2}, \quad (13)$$

where Φ_e is the surface condition number of the e th element and N^d is the total number of dimensions. The surface condition number identifies if an element is located on the boundary surface of a part with large values indicating the element exists on the exterior surface of the part. The surface condition number must be calculated on a domain level in order to identify boundaries that occur where multiple parts would connect from an assembly perspective. The surface condition number of all elements in all part domains is summed to calculate the total surface area in units of element volume, given as

$$\Phi = \tilde{V}^T \Phi, \quad (14)$$

where Φ is the vector of surface condition numbers, \tilde{V} is the vector of element volumes, and Φ is the total surface area.

The direction of the spatial gradient vector provides the inward surface normal and thereby the orientation of the exterior surface of a part, which can be compared to the build direction \hat{b} and the self supporting threshold $\bar{\alpha}$ to determine if support structure is needed at that location. A Heaviside function, $H_{\bar{\alpha}}$ further outlined by Qian [47], is introduced to provide a smooth representation of the discrete change in support requirement when the self-supporting threshold is reached. The supported surface condition number ψ_e is calculated in (15) as the multiplication of

the Heaviside function by the surface condition number to only identify supported elements on the exterior of the part

$$\psi_e = H_{\bar{\alpha}} \left(\frac{\nabla \rho_e}{\|\nabla \rho_e\|} \cdot \hat{b} \right) \Phi_e. \quad (15)$$

A large value of supported surface condition number indicates that an element is on a surface boundary and is overhanging, meaning support material is required. A low value does not require support structure as the element is either on the interior of the part or is built within the specified self-supporting angle.

After supported surfaces are identified, support structure volume is calculated based on a vertical path from the supported surface to either the next surface of the part (the supporting surface) or to the build plate of the part. This approach uses linear supports to provide a reasonable estimate of support structure volume without having to consider complex, custom optimized supports [12, 15]. A peak finding algorithm identifies all surface elements and supported elements along vertical rays throughout each part domain using a specified threshold value. The build plate is identified independently for each part domain as

$$h_d = \min(h_i(\vec{z}_i)) - \Delta \quad \forall \vec{z}_i \in \Omega_d, \quad (16)$$

where h_d is the build plate height of part domain d , \vec{z}_i represents the i th vertical ray belonging to the domain Ω_d , $h_i(\vec{z}_i)$ is height of the lowest surface element identified by the peak finding algorithm in that ray, and Δ represents a small offset accounting for the initial layers of support structure that must be built below the part. Equation (16) identifies the lowest surface in each part domain and adjusts the build plate height accordingly. It is important to adjust the build plate height to accurately calculate the support structure volume when parts begin above the bottom of the design domain. The support volume associated with each supported element can then be calculated as

$$\lambda_e = \int_{a_e}^{b_e} V(\vec{z}_i(t))(1 - \rho(\vec{z}_i(t))) dt, \quad (17)$$

where λ_e is the volume of support material of the e th supported element, $\vec{z}_i(t)$ is the i th parameterized ray with integral quantity t , $V(\vec{z}_i(t))$ is the volume of an element in that ray, $\rho(\vec{z}_i(t))$ is the filtered density of an element along the ray, b_e is the upper integrating limit associated with the supported element, and a_e is the lower integrating limit associated with either the next supporting point or the built plate height of the domain, h_d , calculated in (16). The total support structure volume, Λ , is calculated as the sum of support volume requirements for all N elements as

$$\Lambda = \sum_{e=1}^N \lambda_e . \quad (18)$$

The joint cost can be represented based on the total number of joints and the cost per joint in the assembly. However, the cost per joint is related to the joint type which is often dependant on the industry, application of the part, and the materials used. For these reasons the joint type is considered as a fixed input provided by the user and is not subject to optimization. The joint cost can therefore be represented by the number of joints in the assembly, Γ , and can be calculated as the sum of all design variables in the joining domain as

$$\Gamma = \sum_{j=1}^M y_j . \quad (19)$$

It should be noted that Γ does not represent the actual number of joints required in the assembly as it includes intermediate density finite joint elements. Instead, the parameter can be considered a relative joint cost of the assembly. A more realistic calculation of the number of joints would involve reinterpreting a set of closely packed joint elements as a connection region. A meaningful joint design can be determined through a post-processing step after topology optimization, where parameters such as adhesive bonding area or number of bolts required to avoid failure can be calculated with subsequent finite element analyses using the mechanical properties of desired joint type (adhesive, bolt, weld).

2.3 Sensitivity Analysis

The sensitivity expressions of the objective and constraint functions with respect to both element and joint design variables are required for the use of a gradient based topology optimization solver. The support structure volume and surface area sensitivities are identical to those derived by Ryan et Kim [13] and will therefore not be shown in this work. The sensitivity for these quantities with respect to nodal joint density, y_j , is zero.

The sensitivity of compliance with respect to element design variables is widely available in topology optimization literature as

$$\frac{dC}{dx_e} = -px_e^{p-1} (E_0^1 - E_{\min}) \underline{u}_e^T \underline{K}_e^0 \underline{u}_e , \quad (20)$$

where \underline{u}_e is the displacement vector of the nodes corresponding to element e . The sensitivity of compliance with respect to the nodal joint density can be derived in the same way and represented as

$$\frac{dC}{dy_j} = -qy_j^{q-1} (E_0^2 - E_{\min}) \left(\sum_{c=1}^{L-1} \underline{u}_c^T \underline{K}_c^0 \underline{u}_c \right)_j , \quad (21)$$

where \underline{u}_c represents the displacement vector of all nodes corresponding to connection c of joint j as determined by (7).

The expression for the sensitivity of the total number of joints can trivially be derived as

$$\frac{d\Gamma}{dy_j} = 1 . \quad (22)$$

2.4 Problem Setup

In single-part finite element analysis, forces are specified based on their nodal location in the vector \underline{f} while constraints are identified by eliminating nodal degrees of freedom from the model. The force and constraint nodes correspond directly to their location in the problem definition. In compliance minimization, the initial design variable density of all elements is typically set to the volume fraction defined in the problem statement. When solving a problem using the MLTO approach the standard topology optimization setup must be modified to achieve meaningful results. The proposed process presented in Figure 5 outlines a recommended approach for initializing the MLTO problem and placing boundary conditions throughout the optimization. The initialization process and is explained and justified in detail in the following two sections. Future investigation should be conducted to explore alternate methods that meet the criteria discussed in the following sections.

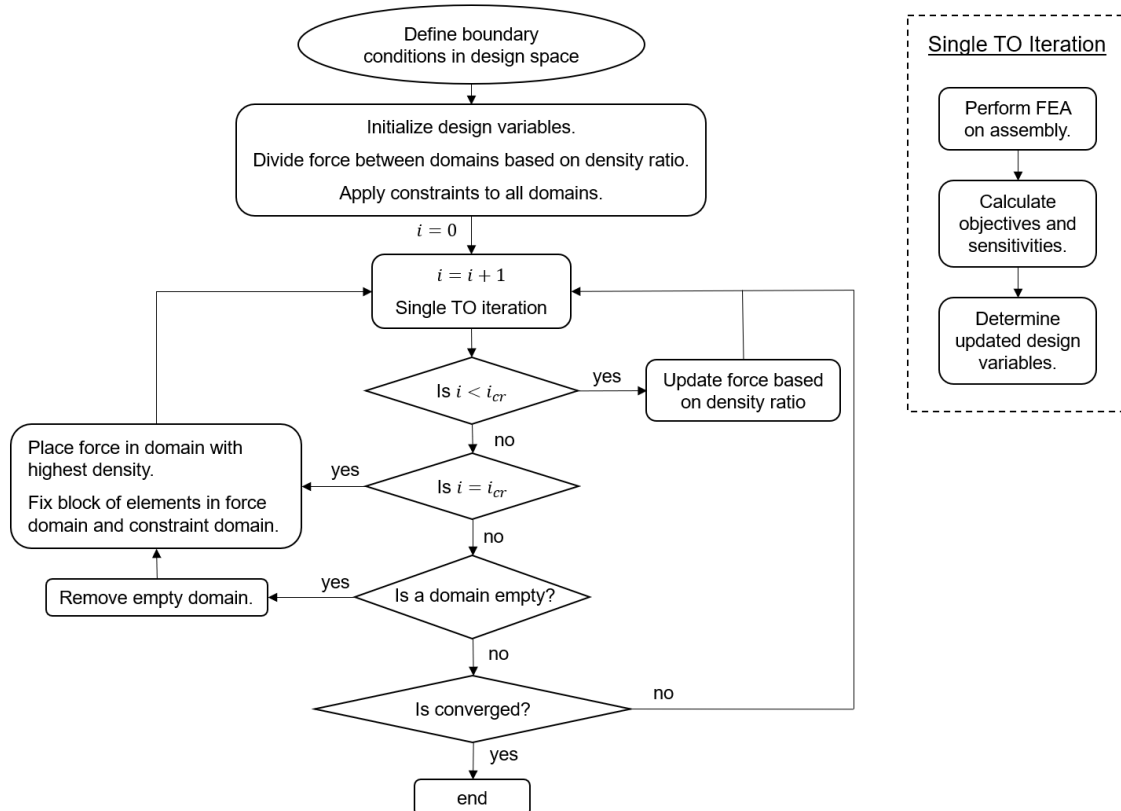


Figure 5: The proposed methodology for placing boundary conditions and fixed elements in MLTO. The process is explained in detail in sections 2.4.1 and 2.4.2.

2.4.1 Boundary Condition Placement

When layered domains overlap, there are multiple nodes occupying the same location, each from different domains. The applied force can not be placed in the respective node of every domain as the sum of the applied forces would be too large. The application of the force and constraint to individual nodes in isolated domains also significantly affect the results of the optimization. For example, if all forces and constraints are placed into a single part domain, the topology optimization will favour a single part design as additional parts are not needed to create a load path between the applied force and constraint nodes. On the other hand, dividing the applied forces evenly into every domain and placing the constraints in a single domain requires L parts to transfer the load from the applied forces to constrained location.

The following principles should therefore be considered for boundary condition definition within the assembly:

1. The boundary condition placement should be as close as possible to the actual loading, particularly after the initial iterations when structural topology is developing.
2. The placement of boundary conditions should not remove design freedom of the assembly or overly influence the convergence towards a certain design. It should be possible to result in a single or multi-part design using the same method of applying boundary conditions only by changing the specified weightings between objectives.
3. Boundary conditions should not be applied directly to a bar element as the purpose of joints is only to connect between domains.

The first criterion can be followed by ensuring that the superposition of all applied forces in each domain is equal to the force specified in the problem definition. The second criterion is more difficult to satisfy as the placement of a force at a node will cause the optimization to place element density at that location. The third criterion can be easily met by creating offsets in the set of feasible nodal joint locations from each boundary condition node.

The proposed technique outlined in Figure 5 splits the applied force at each node between part domains based on the density distribution calculated as

$$f_{i,d} = \frac{\tilde{\rho}_{i,d}}{\sum_{d=1}^L \tilde{\rho}_{i,d}} F_i, \quad (23)$$

where $f_{i,d}$ represents the magnitude of force at the i th node that is split into the d th domain, $\tilde{\rho}_{i,d}$ is the nodal density at the i th node in the d th domain, $\sum_{d=1}^L \tilde{\rho}_{i,d}$ is the total nodal density in all domains at the i th node, and F_i is the original applied force at the i th node defined in the problem definition. The summation of the individual forces is always equal to the original applied force. This method also guarantees that a force will never be placed on an empty node assuming there is element density in at least one domain at that location. Updating the forces between domains based on the surrounding element density ensures the force placement follows the topology of the assembly without forcing element density into any one individual part domain.

After initializing the applied force, the constraints from the problem statement are applied to all part domains. Unlike an applied force, constraints can be placed in all domains as they do not require the placement of material at that node. The optimization proceeds for a set number of iterations, i_{cr} , updating the force based on the density ratio after each iteration. After the critical iteration (in this case $i_{cr} = 3$), the full magnitude of the force is placed in the domain with the highest nodal density and a block of solid elements with a length equal to the filter radius is placed around the force node to avoid a singular finite element problem [48]. A similar block of elements is placed in the domains with the greatest element density at each constraint location, except for constraints representing symmetry planes.

This approach allows for development of the number of parts and the part geometry in the initial iterations without any restrictions on design freedom. After the force is placed in the critical iteration, design freedom is lowered, but the boundary conditions more closely match the problem statement. The usage of each part domain is monitored throughout the optimization and unused domains (defined as an average element density of less than 0.005 for 5 consecutive iterations) and their associated design variables and degrees of freedom are removed. After a domain is removed, the placement of the applied load is recalculated, and fixed element blocks are placed in new locations based on the maximum nodal density at each boundary condition location.

2.4.2 Design Variable Initialization

With multiple domains, the simplest design variable initialization would be to set all element densities to the same value calculated as

$$\rho_{init} = \gamma / L, \quad (24)$$

where ρ_{init} is the initial element density that satisfies the volume fraction constraint, as it is generally recommended to begin an optimization without any constraint violation for best convergence. However, if all part domains have the same initial element density, the boundary condition method described above will split the applied force evenly between all domains, causing the element sensitivities fields of each domain to be identical. Therefore, all design modifications will in turn be uniform between domains for each iteration. This will result in identical part geometries in each domain as there is no driving factor to differentiate between part domains. After the placement of the force in the critical iteration, this initialization would eventually converge to a single part design. This behaviour is prohibitive to assembly design as the equivalent sensitivities prevent the development of unique parts between domains.

This convergence problem can be avoided by introducing a unique initial density distribution for each part domain. This distribution should be significant enough to result in the formation of unique parts between domains, but not too large that it makes it impossible to converge to a single part design. The average density in each domain should be equal to ρ_{init} defined in (24) to ensure that each domain is equally favoured. A smooth density gradient such as the one shown in Figure 6 can be applied to each domain, with a higher density originating at one end of a domain transitioning to a lower density at the opposite end of the domain. This gradient initialization method causes a small bias towards one side of a domain but still allows for the development of

density at any location. It should also be noted that the penalty factor must be sufficiently large ($p > 2$) in initial iterations to encourage the formation of multiple unique parts.

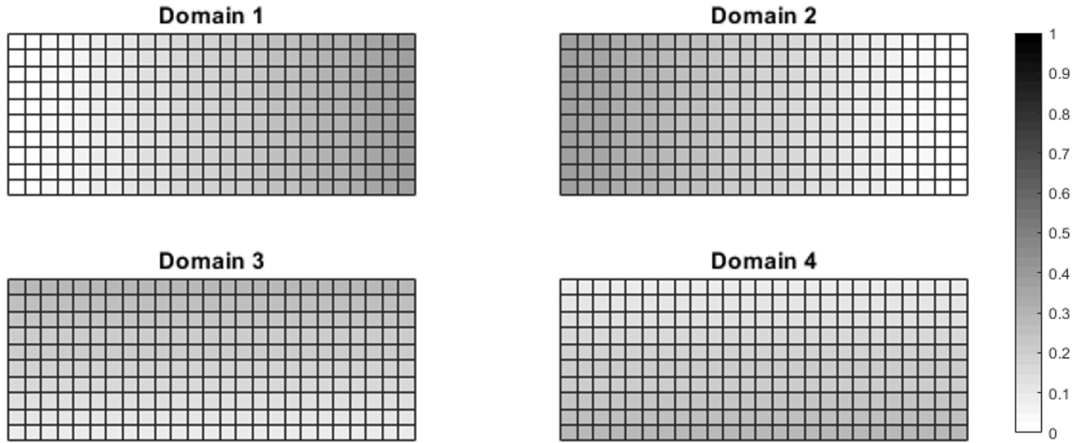


Figure 6: A sample gradient distribution of initial density between four domains using a 75% volume fraction and 25 \times 10 elements for visualisation purposes. Paired domains with opposing gradients ensure an even distribution of material on the assembly level for the first iteration.

It is also important that the density distribution on the domain level does not limit the placement of density globally at the assembly level. In other words, an equal amount of density should be placed at each element location in the original design space (among all part domains). By pairing two domains together and applying opposing gradients to the initial density distribution, the sum of the density in each pair will always result in a uniform density distribution, removing any bias at the assembly level. This is demonstrated in Figure 6 where domains 1-2 and 3-4 are respectively paired together with opposing gradients.

The magnitude of the gradient can be changed to alter the “strength” of the bias towards one location within a domain. The direction of the gradient can also be specified to determine which locations within the domain are given a bias. Combinations of horizontal and vertical gradients with different magnitudes can generate gradients of any direction and magnitude. In Figure 6, domains 1 and 2 transition horizontally between a density of 0 and $2\gamma/L$ while domains 3 and 4 transition vertically between densities of $\gamma/2L$ to $3\gamma/2L$.

It is evident that the selection of the direction and magnitude of the gradient will have a significant impact on the optimized design as it inherently favours a single location in each domain. Investigation into the impact of design variable initialization on the final design as well as development of different methodologies for problem setup will be left as future work.

The initialization of joint density is another important consideration, but there is no constraint limiting the number of joints and therefore no corresponding starting joint density to satisfy that constraint. A parameter study indicated that assembly designs were favored when joints were all initialized with initial joint densities close to $y_{init} = 1$, while single part designs were more likely to occur with values close to $y_{init} = 0$. From the results of a parameter study, the joint density in

the first iteration is linearly interpolated between y_{init}^{\min} and y_{init}^{\max} based on the ratio of weighting factors that are applied to joint objective as shown in (25). These parameters were set to $y_{init}^{\min} = 0.05$ and $y_{init}^{\max} = 0.15$ for 2D problems and were set to $y_{init}^{\min} = 0.15$ and $y_{init}^{\max} = 0.90$ for 3D problems.

$$y_{init} = y_{init}^{\min} + \left(y_{init}^{\max} - y_{init}^{\min} \right) \left(1 - (1 - w_1) w_2 \right). \quad (25)$$

3 NUMERICAL EXAMPLES AND RESULTS

The proposed MLTO algorithm was implemented in a custom MATLAB topology optimization code. The method of moving asymptotes proposed by Svanberg [49] was used as the gradient based optimization algorithm, with the move limits decreased to 0.125 to improve initial convergence behavior. A three-phase adaptive penalty scheme was implemented where the element penalty factor is incremented from $p = 3$ to $p = 4$ (and later $p = 5$) after a convergence criteria of 2% change in all objective functions was met over the previous 5 iterations. This encourages element density to approach more discrete solutions, which can be challenging when minimizing surface area and support structure. An alternative approach for achieving more discrete results is the projection method proposed by Wang et al. [50], which gradually increases the slope of a projection scheme to encourage discrete density results. The resultant element densities were thresholded using a volume-preserving bisection algorithm and joint densities were thresholded to 0 or 1 with a threshold value of 0.5.

The three load cases presented in Figure 7 were applied to validate the MLTO approach. The 2D design domains were discretized into 250×100 square elements while the 3D design space was discretized into $60 \times 40 \times 30$ square elements, all of length 1 mm. The domain extension approach proposed by Clausen and Andreassen [48] was employed to ensure accurate density gradient calculations on the exterior borders. The material Young's modulus was set to $E_0^1 = 200$ GPa with a Poisson's ratio of $\nu = 0.3$ and a base joint stiffness of $E_0^2 = 2000$ N/mm was used. A self-supporting threshold of 45 degrees was used for supported surface calculations. Objective function values were normalized with the initial function values after problem initialization, except for surface area (which was normalized with the perimeter of the design space) and support structure volume (which was normalized with the volume of void material in the design space as $\Lambda_0 = (1 - \gamma) V_0$). The presented problems use simple geometries with structured meshes, however the methodology and code implementation can be extended for more complex problems with unstructured meshes in future work.

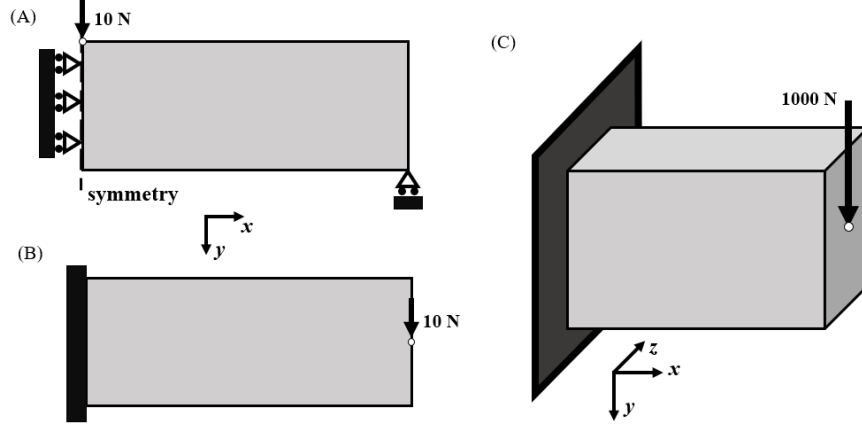


Figure 7: 2D and 3D test problems outlining the design domain, constraints and applied forces. (A) represents a 2D Messerschmitt-Bolkow-Blohm beam, (B) outlines a 2D cantilever beam, and (C) outlines a 3D cantilever beam.

The two load cases were solved using four part domains to provide increased design freedom with the MLTO approach. A further increase in the number of part domains would in turn increase design freedom but would require added computational cost as the size of the finite element matrix grows larger. The 3D test problem was instead solved using two part domains to reduce computational costs. The initial element density gradient applied to both problems is shown in Figure 8. A diagonal gradient distribution was found to generate favourable assembly designs as it encouraged a part to form in the corner of each domain. The 3D problem with two domains used a uniform density gradient from the fixed face to the face with the applied force. The build plates are represented with a blue line and the height of the build plate is adjusted throughout the optimization. The print direction for each domain is represented by a red arrow, each of which were manually selected at the beginning of the optimization based on the initial density distribution and the expected topology of the structure. A poor selection of print direction may result in increased support structure volume when compared to a single part, eliminating the reduction in printing costs when consolidating a design. Ideally, a unique print direction should be calculated throughout the topology optimization process for each domain.

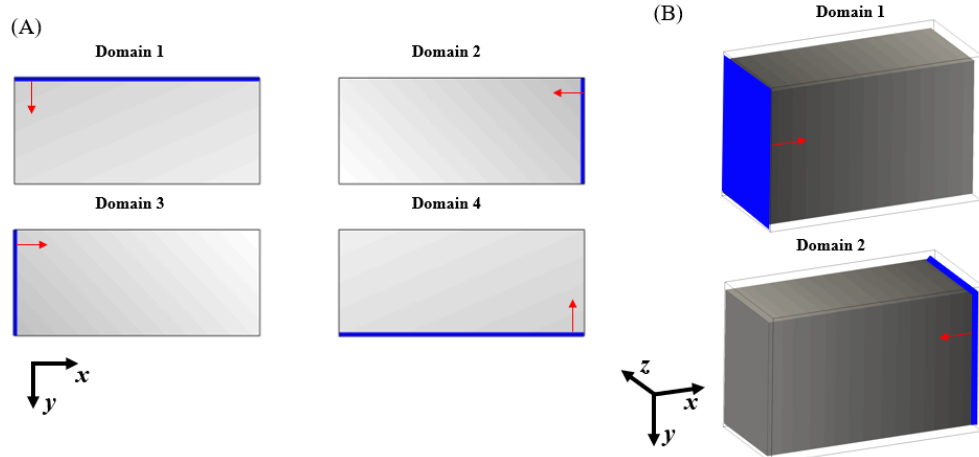


Figure 8: Initial element density distribution used in (A) 2D problems and (B) the 3D problem. Blue lines indicate the build plate in the first iteration and the red arrows indicate the print direction.

3.1 Messerschmitt-Bolkow-Blohm Beam

3.1.1 Joint Minimization

To verify that the proposed MLTO algorithm is capable of consolidating an assembly into a single part, designs were optimized for a joint cost weighing of $w_2 = 1$ and structural-cost weightings between $w_1 = 0.2$ and $w_1 = 0.99$ with a volume fraction of $\gamma = 0.3$. These weightings remove all additive manufacturing costs from the optimization problem statement and minimize the weighted sum of compliance and the number of joints. The material parameters used in the optimization ($E_0^1 = 200 \text{ GPa}$, $E_0^2 = 2000 \text{ N/mm}$) result in a significantly lower joint stiffness when compared to element stiffness. An assembly design would therefore result in higher structural compliance when compared to a single part design as the load would need to transfer between the low stiffness joints instead of the part material. When only maximizing structural performance and minimizing the number of joints, the optimal solution should therefore result in a single part without joints. However, when loads are transferred between multiple part domains, increasing the number of joints will decrease the compliance as it strengthens the connection between those parts. In other words, there are conflicting objective sensitivities outlined in equations (21)-(22) and the optimization may not converge to a single part design depending on the weighting factors between objectives. The base joint stiffness also affects the ratio between the conflicting sensitivities and a reduction in joint stiffness would also lead towards a single part design.

The number of joints and parts in the optimized MBB designs plotted in Figure 9 indicate that decreasing w_1 results in a reduction of joints in the optimized assembly design. The reduction in joints is also accompanied by a decrease in the number of parts as w_1 is reduced. These results confirm that the MLTO approach has the design freedom to converge to single or multi-part design by varying the associated weighting factors.

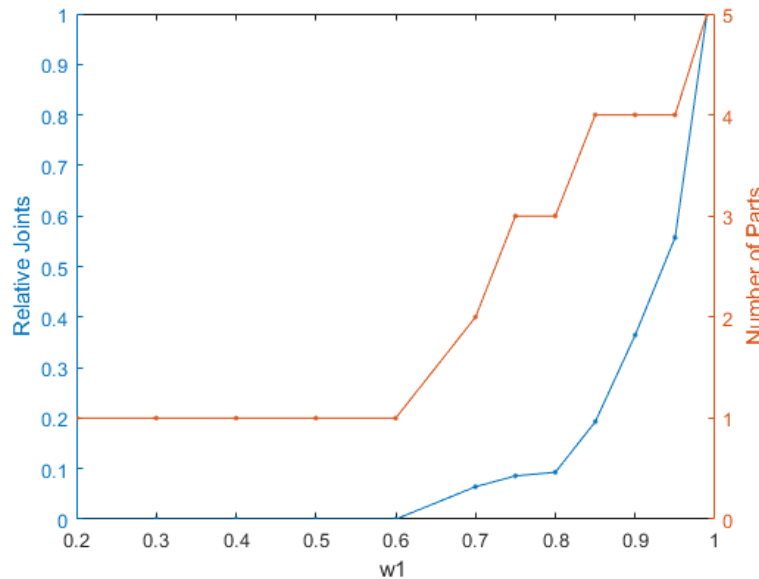


Figure 9: The number of joints and parts in optimized design as the structural-cost weighting is varied for the MBB beam problem with no AM cost weightings.

Resultant assembly designs from this optimization are presented in Figure 10 including a plot of individual part and joint densities, along with a representation of the combined assembly design. Joints are plotted in each part domain (if element density exists at that location) with a purple marker if the connection originated from that respective domain, or a green marker if the joint originated from another domain. Joints are connected to every domain based on the connection pattern outlined in (7), but are only plotted if element density exists in the respective domain for simple visualisation. All joints are plotted only once with red markers in the assembly design.

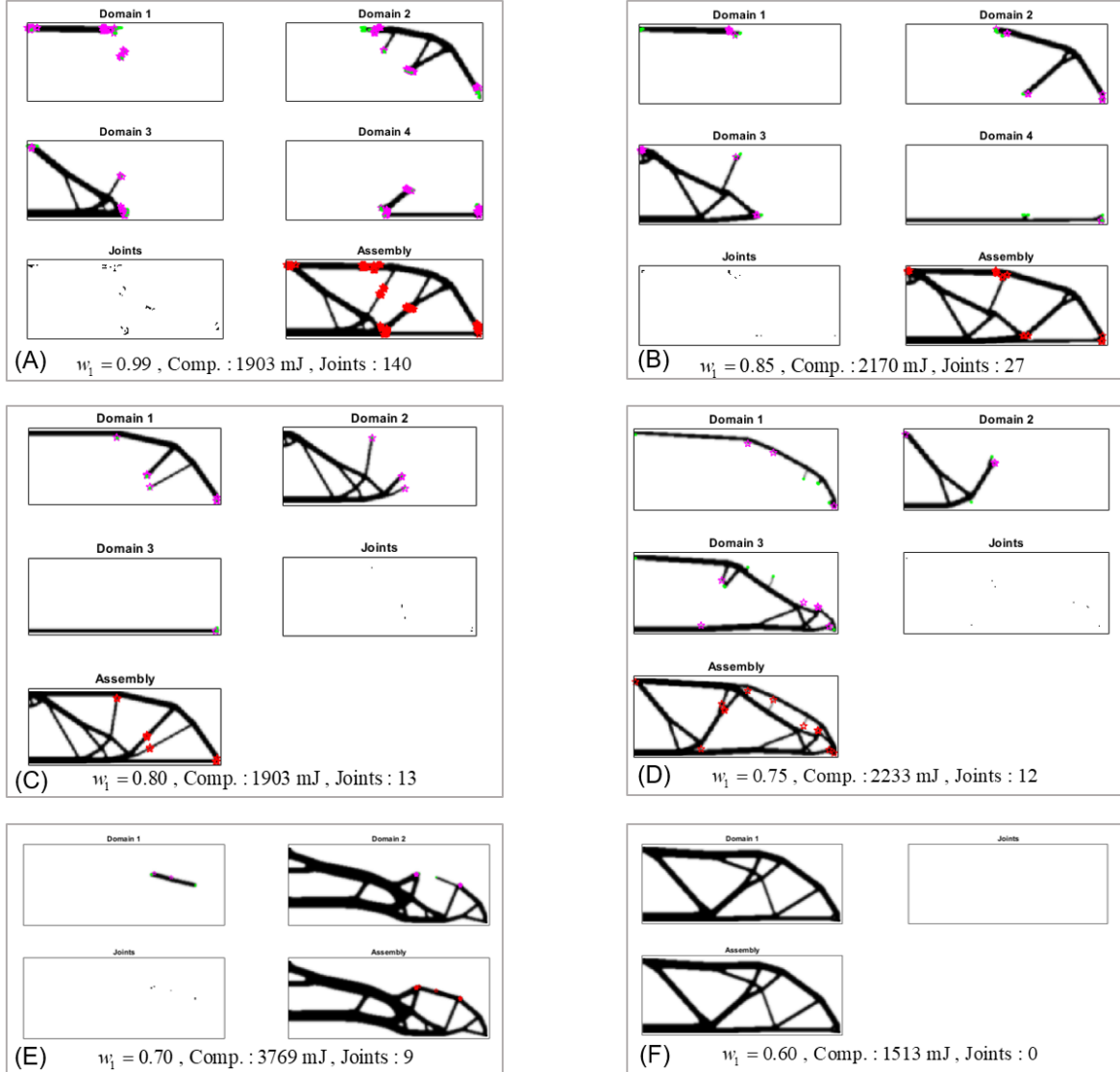


Figure 10: Optimized MBB beam assembly designs for compliance and joint minimization with various structural-cost weightings.

These designs show that the MLTO approach places joints only at the connection points between parts. As the focus of the optimization shifts towards minimizing joints, the final structural topology generally results in less overall connection locations between parts as shown in designs (A) and (B). As w_1 continues to decrease, the number of parts in the assembly are gradually reduced

as shown in designs (B) to (C) and designs (D) to (E). This demonstrates that the approach is not only capable of minimizing the number of joints but can also indirectly reduce the number of parts. The optimization results in a fully consolidated single-part design for a structural-cost weighting of $w_1 = 0.6$.

A small change in the w_1 weighting results in a minor change to assembly topology that reduces the number of connections while keeping the same number of parts, as shown from designs (A) to (B). A large change in w_1 results in a change in how the assembly is divided to decrease the part count, as shown between designs (A) and (C). Another important observation is that the assembly-level designs all share similar major load paths except in Figure 10 (E) where the optimization converges to a poor local minimum point.

The assembly design in Figure 10 (F) is the ideal solution of the presented designs when only considering compliance and joint objectives. All other designs were sub-optimal due to the conflicting sensitivity values of joint design variables and the potential for falling into a local minimum objective function region with a gradient based solver. However, when AM part costs are accounted for in the optimization, an array of optimized solutions will exist depending on the desired trade-offs between joint cost and part cost.

3.1.2 Joint, Support Volume, and Surface Area Minimization

In this section, the full MLTO problem statement is applied with simultaneous optimization of compliance, joints, support volume, and surface area for a volume fraction of $\gamma = 0.3$. The support volume to surface area weighting is left fixed at $w_3 = 0.9$ as this was found to improve objective convergence by smoothing part boundaries. The structural-cost weighting was varied from $w_1 = 0.5$ to $w_1 = 0.99$ for five joint-part cost weightings of $w_2 = 0.1, 0.3, 0.5, 0.7, 0.9$.

The optimization progress between iterations is presented in Figure 11 for a baseline assembly design with minimal AM and joint cost weightings of $w_1 = 0.99$ and $w_2 = 0.50$. These snapshots outline the convergence from the initial conditions to the final assembly design. The initial element density gradient evolves into a density distribution similar to a traditional topology optimization in iteration 10 but with the element densities split into four separate domains. Two blocks of solid elements are placed after the critical iteration ($i_{cr} = 3$) indicating that the largest density near the applied force and roller constraint occurred in domains 1 and 4 respectively. The unconnected element density in other domains at the boundary condition area disappears by iteration 10 as shown in the bottom right-hand corner in domains 1 and 3, and the top left-hand corner in domains 2 and 4.

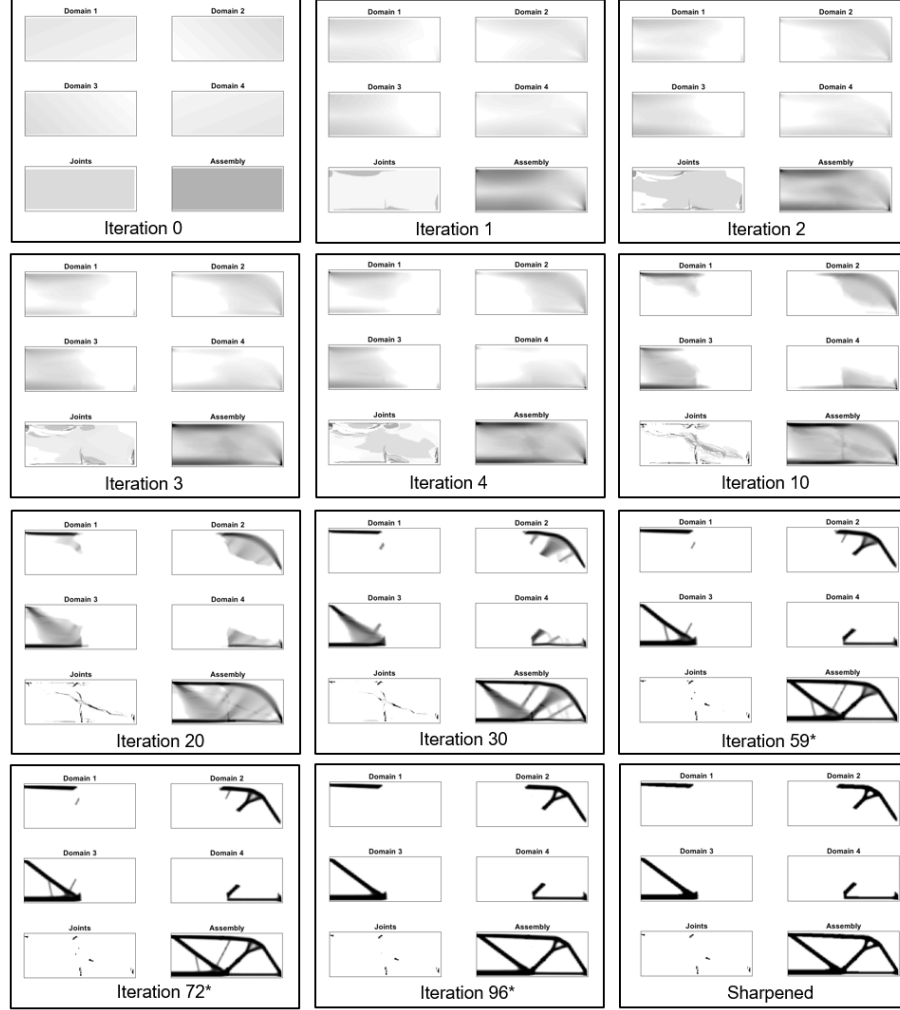


Figure 11: Optimization history of the MLTO process for the MBB beam problem with a small weighting for cost minimization ($w_1 = 0.99$, $w_2 = 0.50$)

The distribution of joints varies significantly between initial iterations as the element densities and connection between parts is not clearly defined. After the location of the part within each domain is solidified in iteration 10, joints are located entirely along the boundary edges between parts. The total number of joints is gradually reduced after iteration 10 with joints eventually placed only at interfaces between parts as the individual part topology is refined. An asterisk is placed by the iteration number when each of the three phases converged. The geometry of the part is almost entirely decided after the first phase, while the second and third phases mainly reduce intermediate element densities due to the increase in element penalty factor. The sharpened assembly represents the final thresholded element and joint densities. Implementing the density projection scheme proposed in [50] is a potential solution for assisting in convergence to a discrete solution while avoiding nonlinearly at the start of the optimization. Optimization history of the four objective functions values (compliance, joints, support structure volume, and surface area) is presented in Figure 12. The compliance objective starts relatively large due to the very low element densities in all domains and decreases rapidly after as the design converges. The number of joints also has

significant fluctuations in early iterations as the geometry is being split into parts. Surface area and support structure volume have values of zero in initial iterations because the boundaries of the part are not clearly defined. As the optimization progress and the interfaces and overhangs appear, these objective function values gradually increase. The change in slope of surface area convergence (which also appears in compliance and joint objectives at a smaller scale) is associated with the change in the SIMP penalty factor in the multi-phase approach.

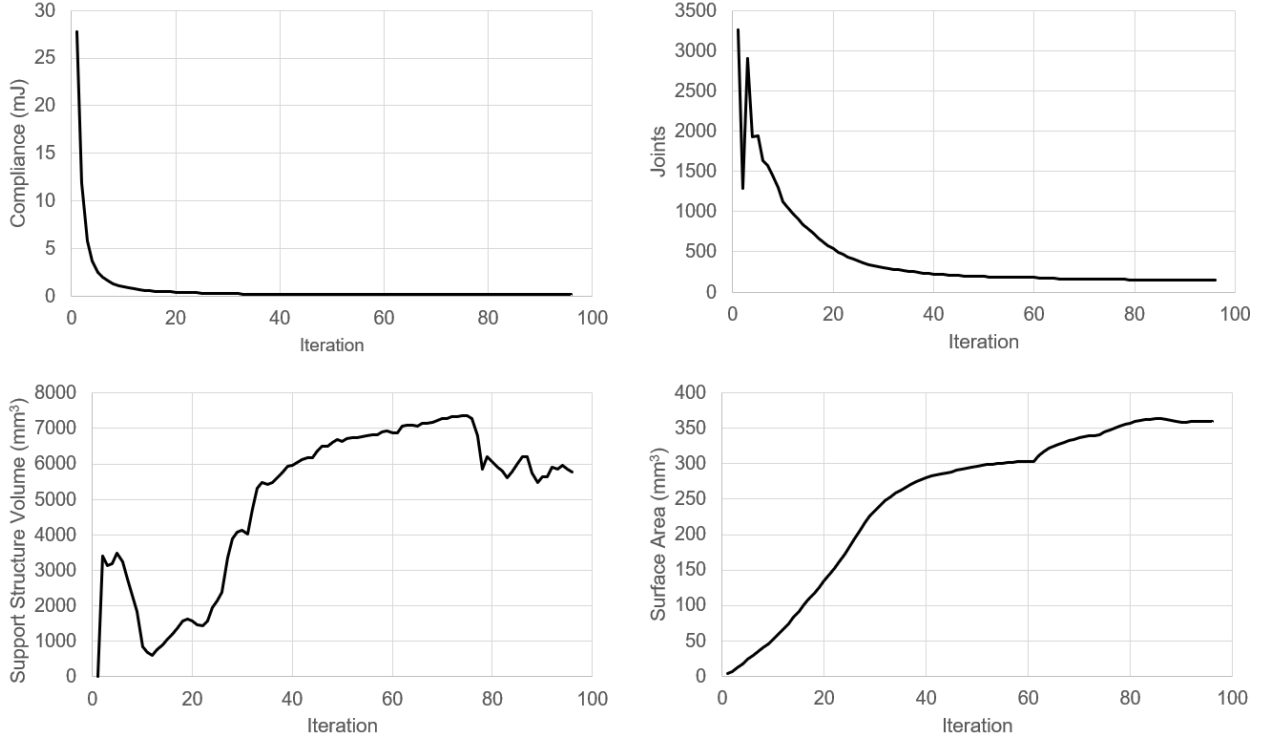


Figure 12: Objective function history for the MBB beam optimization with a small weighting on cost ($w_1 = 0.99$, $w_2 = 0.50$).

Figure 13 presents the optimization history when weighting factors are selected to favor a reduction in joints ($w_1 = 0.60$, $w_2 = 0.90$). A major change from the previous example is apparent in iteration 1 where the joint density is very close to zero for all locations. Joint densities fluctuate over the next 2 iterations, eventually converging to a low number of joints by the fourth iteration. While joint densities are fluctuating, element densities move towards a single domain due to the low connection strength. After the fourth iteration, the applied force can be transferred to the constraint entirely through domain 4. Essentially all element density is removed from the other three domains by iteration 8 and the empty domains are removed by iteration 13. After this point, the optimization proceeds as a single-part topology optimization as the joint design variables remain at zero for the remaining iterations. Objective function history shown in Figure 14 shows the large variations in objective values in early iterations, followed by smooth convergence after a single part design is selected. It is evident from these two examples that the convergence of the initial 10 iterations has a large influence on the number of parts in the final design, and the choice of boundary conditions and initial densities are therefore crucial to the MLTO approach.

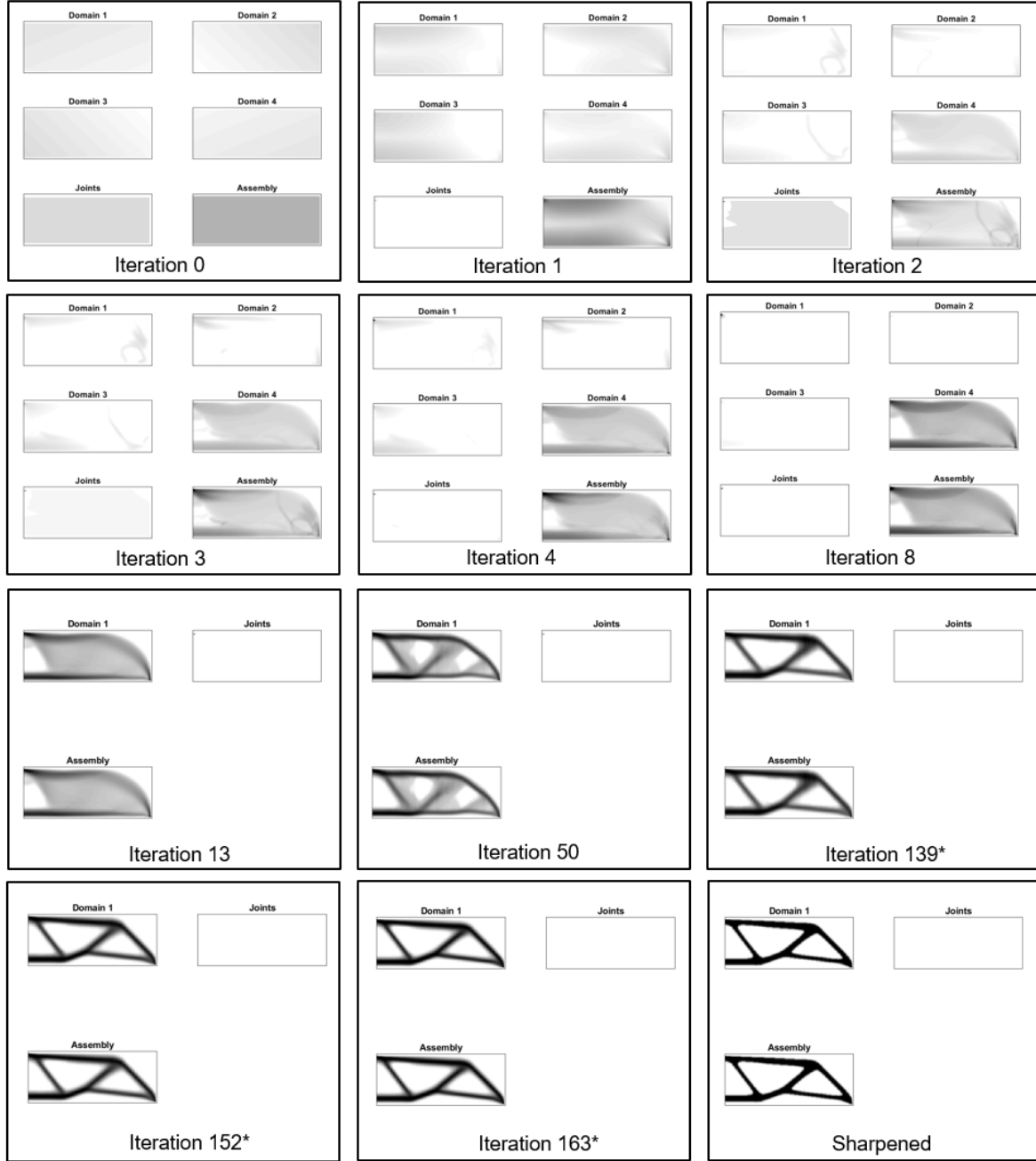


Figure 13: Optimization history of the MLTO process for the MBB beam problem with a focus on joint minimization ($w_1 = 0.60$, $w_2 = 0.90$).

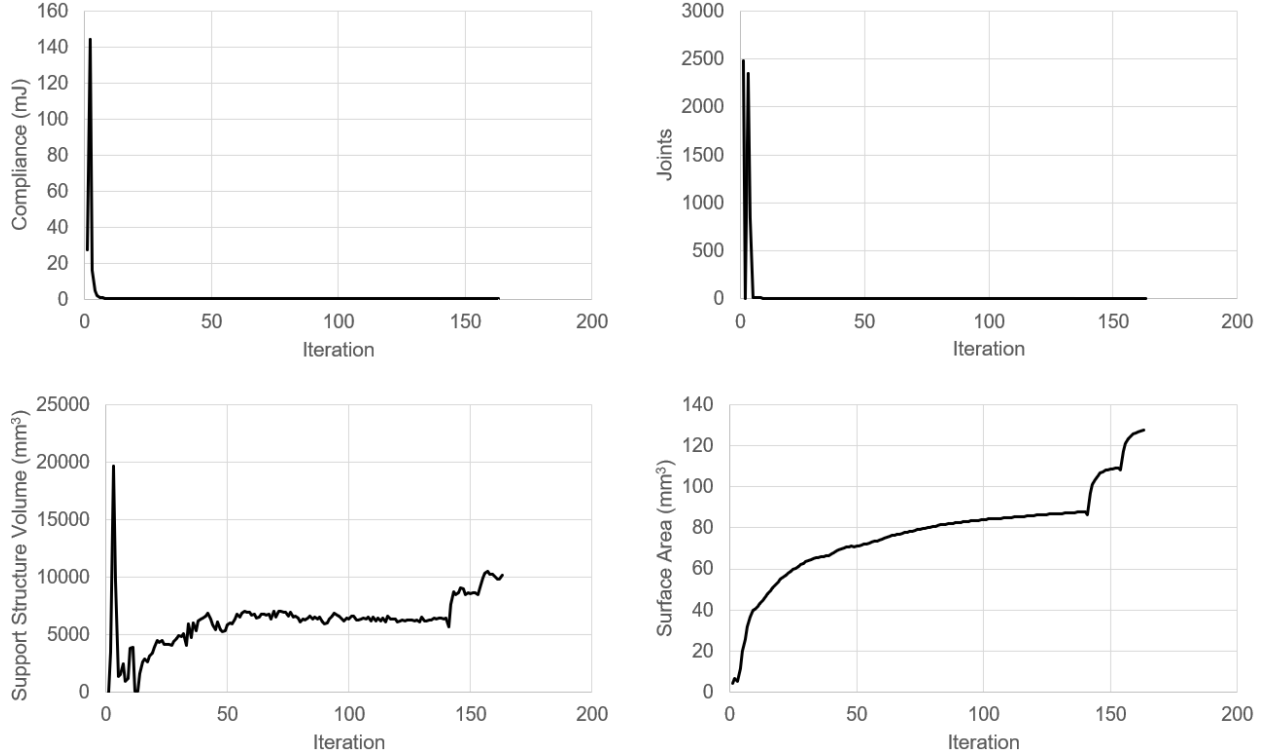


Figure 14: Objective function history for the MBB beam optimization with a large weighting on joint cost ($w_1 = 0.60$, $w_2 = 0.90$).

The optimization history resulting from weighting factors selected to minimize support structure volume ($w_1 = 0.80$, $w_2 = 0.10$) is presented in Figure 15. The initial 10 iterations behave similarly to the baseline assembly in Figure 11 as there are similar weighting factors on minimizing joints. A large change in structural topology occurs between iterations 30 and iteration 261 in domain 3, where the optimization ‘pulls’ the 45-degree member towards the build plate to reduce the associated support structure volume requirements. This results in a sharp increase in structural compliance that is deemed acceptable by the optimizer due to the high weighting on AM cost factors. The optimization process requires significantly more iterations to reach convergence, shown in the plots of objective function history in Figure 16, when large weightings are placed on support structure minimization. This effect was acknowledged by Ryan and Kim [13] and occurs when surface orientation falls close to the self supporting threshold angle causing unstable support structure volume calculation.

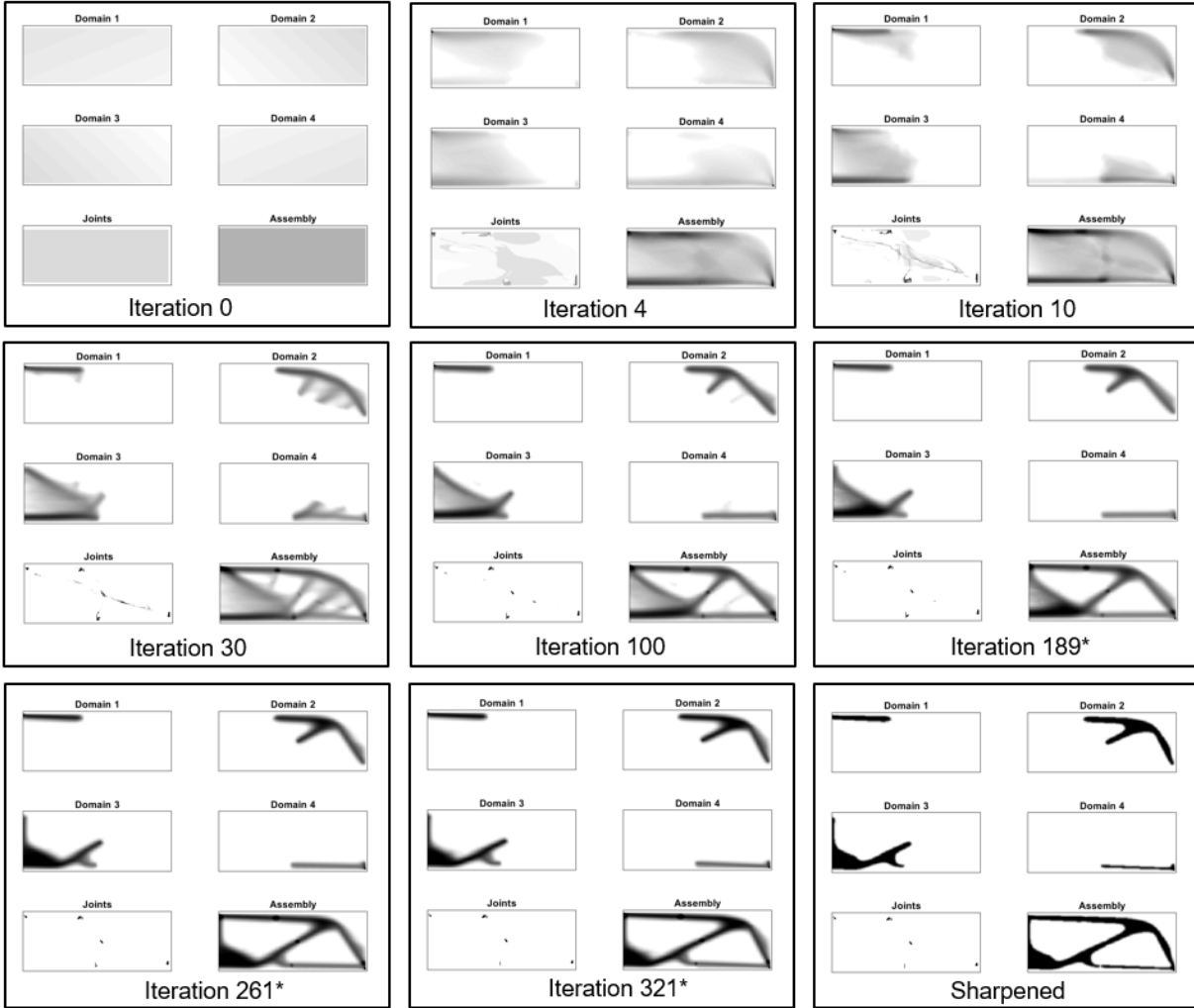


Figure 15: Optimization history of the MLTO process for the MBB beam problem with a focus on support structure volume minimization ($w_1 = 0.80$, $w_2 = 0.10$).

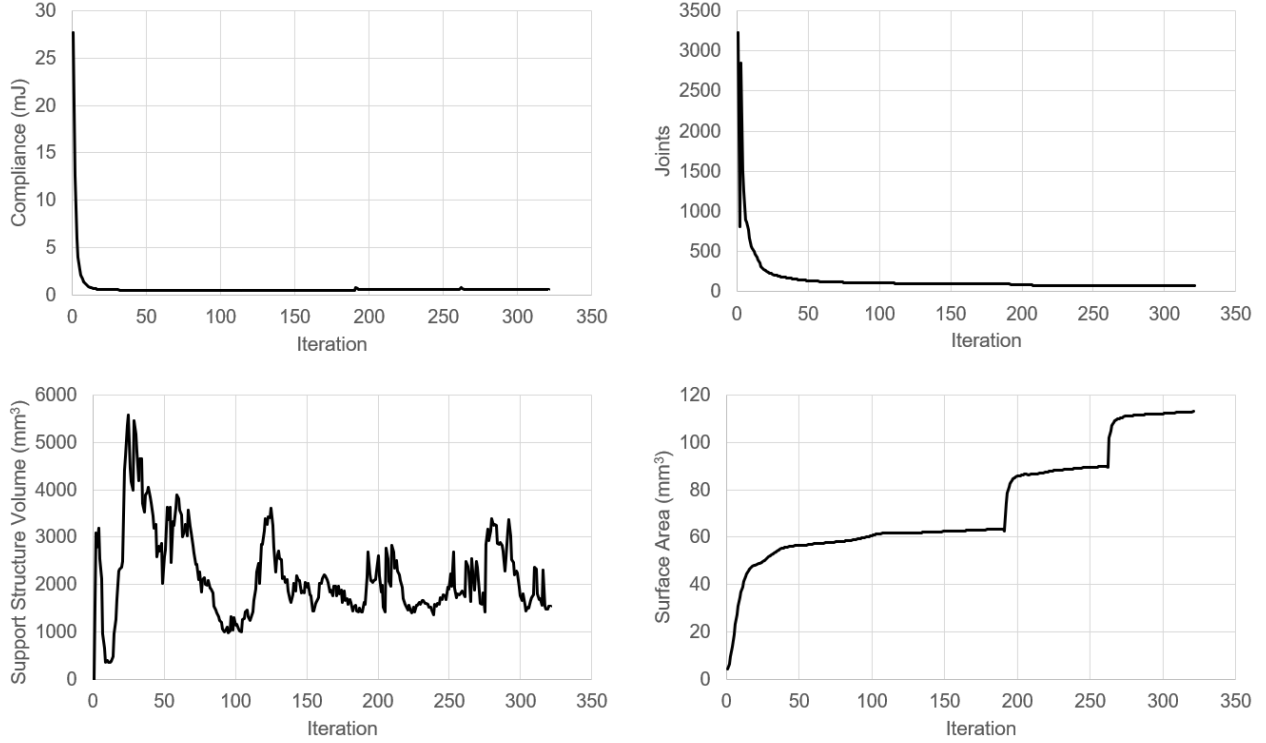


Figure 16: Objective function history for the MBB beam optimization with a large weighting on part cost ($w_1 = 0.80$, $w_2 = 0.10$).

A summary of objective values for select designs generated by the MLTO approach are presented in Figure 17 along with baseline topology optimization results. The baseline single part shown in Figure 17 (A) and the baseline assembly design shown in Figure 17 (C) both have little to no weighting applied to AM and assembly cost factors. The compliance, support volume, and surface area objectives are measured relative to the single part topology optimization solution while the number of joints is measured relative to the baseline assembly to provide an easy comparison between objectives.

A comparison between the two baselines shows that the assembly design yielded a 60% decrease in support structure volume with only a 12% increase in compliance. This reduction in support volume was achieved only by considering an assembly instead of a single part design, without including additive manufacturing cost factors in the optimization problem statement. When the AM cost factors are included, the design shown in Figure 17 (D) has an 87% decrease in support structure volume at the cost of a 114% increase in compliance of the baseline single part. The 52% reduction in joints between designs in (C) and (D) is partially responsible for the large increase in compliance that occurs. The number of connections between parts remains constant while the number of joints has decreased, resulting in an overall reduction in strength at each connection. The design shown in Figure 17 (B) with a focus on joint minimization is similar to the baseline single part with a 12% increase in compliance and comparable support volume, but a 24% reduction in surface area. A change in print orientation would likely result in a more favourable support volume requirement for this design. These results outline that there is a complex

relationship between each of the problem objectives and that the MLTO approach can provide a wide range of solutions based on the selected weighting factors.

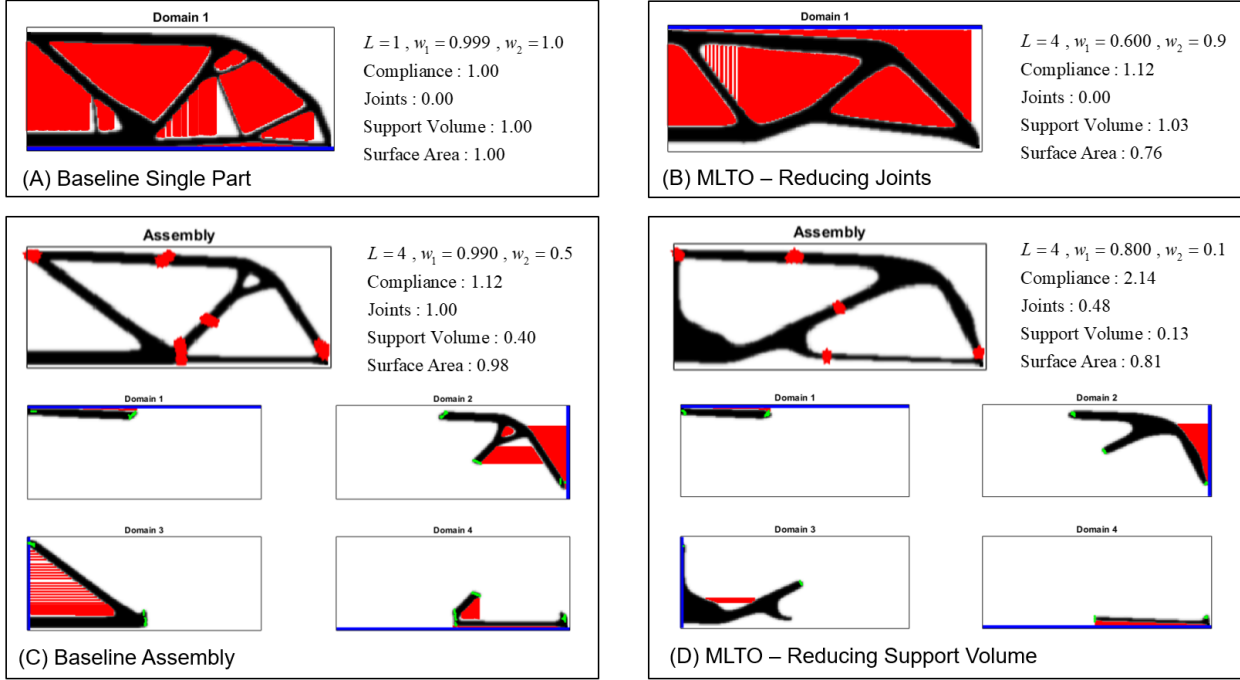


Figure 17: Summary of multi-objective optimization outlining the results producing the lowest support structure volume and lowest number of joints for the MBB beam problem. (A) and (C) outline the baseline single part and assembly designs, while (B) and (D) provide the optimized designs for their respective cost trade-offs.

In order to analyze the relationship and potential trade-offs between design objectives, plots of objective function values across the parameter sweep are presented in Figure 18. Each coloured line represents a fixed joint-part cost weighting factor (w_2) optimized for a sweep of structural-cost weightings (w_1) with objectives measured relative to the baseline designs from Figure 17. Only optimal solutions generated by the parameter sweep in terms of compliance, support volume, and number of joints are included in the plots.

Figure 18 (A) represents a 3D plot of support structure volume, compliance, and number of joints along each w_2 weighting showing the complex relationship between objective functions. A reduction in the w_1 weighting typically results in an increase in structural compliance and a reduction in cost factors. However, the resultant change in individual cost factors (support volume, surface area, number of joints) varies significantly based on the w_2 weighting. A w_2 factor close to zero results in a decrease in support structure and joints with a large increase in compliance, while a w_2 factor close to one results in a large decrease in joints with increases or decreases to support volume and compliance.

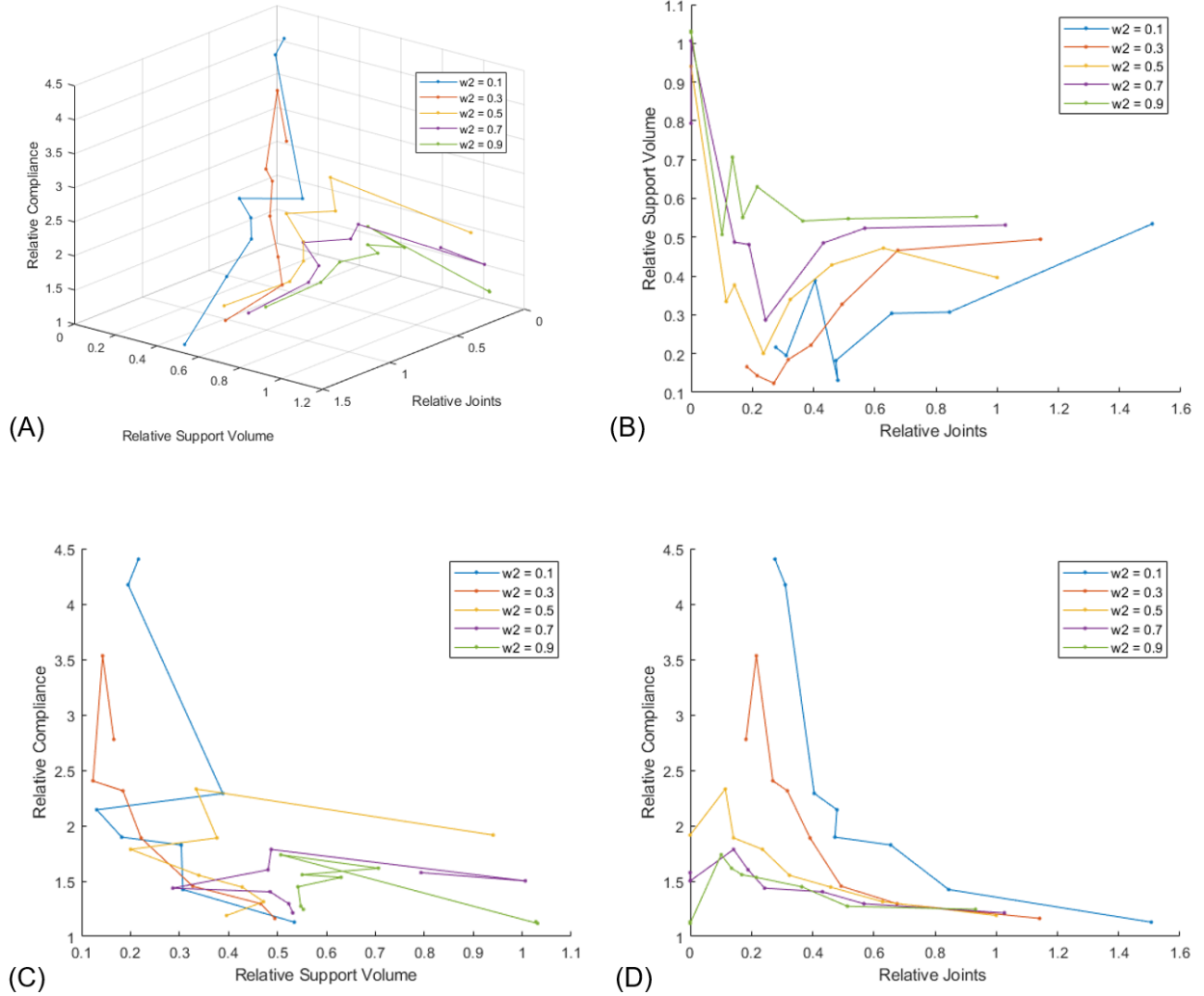


Figure 18: Visualization of parametric study results for minimization of relative support structure volume, joints, and compliance for the MBB beam test case with a 30% volume fraction. (A) plots the results for all weighting values in three dimensions indicating the trade-off between all objectives. (B)-(D) show 2D plane views of the results to compare the performance of only two objectives.

Figure 18 (B) - (D) shows side views of the 3D results projected onto one plane to isolate the relationship between two objective functions. It is important to note that direct conclusions on the relationship between two objectives can not be drawn when looking at a 2D representation of the 3D results because the third objective is not held constant.

Figure 18 (B) outlines the relationship between the relative number of joints and support structure volume in the optimized designs. For low w_2 cost weightings, both joints and support volume are simultaneously minimized, however the optimizer was not able to produce a design without joints. For high w_2 weightings, there is a clear trade-off between objectives as the support structure volume increases after the number of joints in the assembly is reduced. The overall trend indicates that in this instance, both joints and support structure volume can be minimized up to a critical point, after which the decrease in joints results in a large increase in support structure volume. This

large increase in support structure volume is associated with a reduction in the number of parts in the assembly. In some cases, support volume was reduced by approximately 85% by avoiding a full consolidation to a single part. By considering both objectives when optimizing a consolidated design, the total cost can be minimized based on the specified trade-offs between costs.

Figure 18 (C) indicates that support structure volume was effectively minimized for low joint-part cost weightings ($w_2 = 0.1$ and $w_2 = 0.3$) with an associated increase in compliance. Support volume minimization was most effective with a structural weighting near $w_1 = 0.8$, as both compliance and support structure volume increased past this value. A reduction in support structure volume is no longer apparent after joining costs increase ($w_2 > 0.3$) and the objective priority shifts towards minimizing joints. In some instances, minimizing the total cost resulted in an increase in support volume as the associated decrease in joints outweighed the increase in AM costs.

The comparison of joints and compliance in Figure 18 (D) indicates that there is an increase in compliance associated with a decrease in joints when the number of parts remains constant (such as when $w_2 = 0.1$). However, if a higher weighting on joint cost causes the number of parts to decrease, the compliance remains constant or can decrease in some cases with the reduction in joint cost. This plot has a minimum point when the $w_2 = 0.9$ line intersects the relative compliance axis, indicating a single part without any joints. There is therefore not always a clear trade-off between joints and structural performance, particularly when using joints with low stiffness.

The support structure-surface area weighting was held constant at a value of $w_3 = 0.9$ as the effects of direct surface area minimization were previously investigated by Ryan and Kim [13]. The relationship between surface area and other design objectives is presented in Figure 19. A decrease in surface area is associated with an increase in compliance in Figure 19 (A) when the number of parts in the optimized design remains constant with $w_2 = 0.1 - 0.3$. This relationship is no longer observed when the number of parts changes for a constant w_2 weighting, as a reduction in number of parts may reduce both surface area and compliance. However, it is important to note that the increase in compliance that occurs is in large part due to the reduction in other cost factors such as support volume and joint minimization.

Figure 19 (B) indicates that the number of joints and surface area are not conflicting objectives as both decreased simultaneously as the w_1 is lowered. A possible explanation for this link is that under the MLTO formulation, a connection area will always require both a joint and an overlapping area between 2 parts that increases the overall surface area of the assembly. Reducing the number of connections decreases the number of joints and the amount of overlaps present, in turn reducing the total surface area of the assembly. No evident relationships can be drawn by comparing support volume and surface area in Figure 19 (C), indicating that it is unlikely that a trade-off exists between the two objectives.

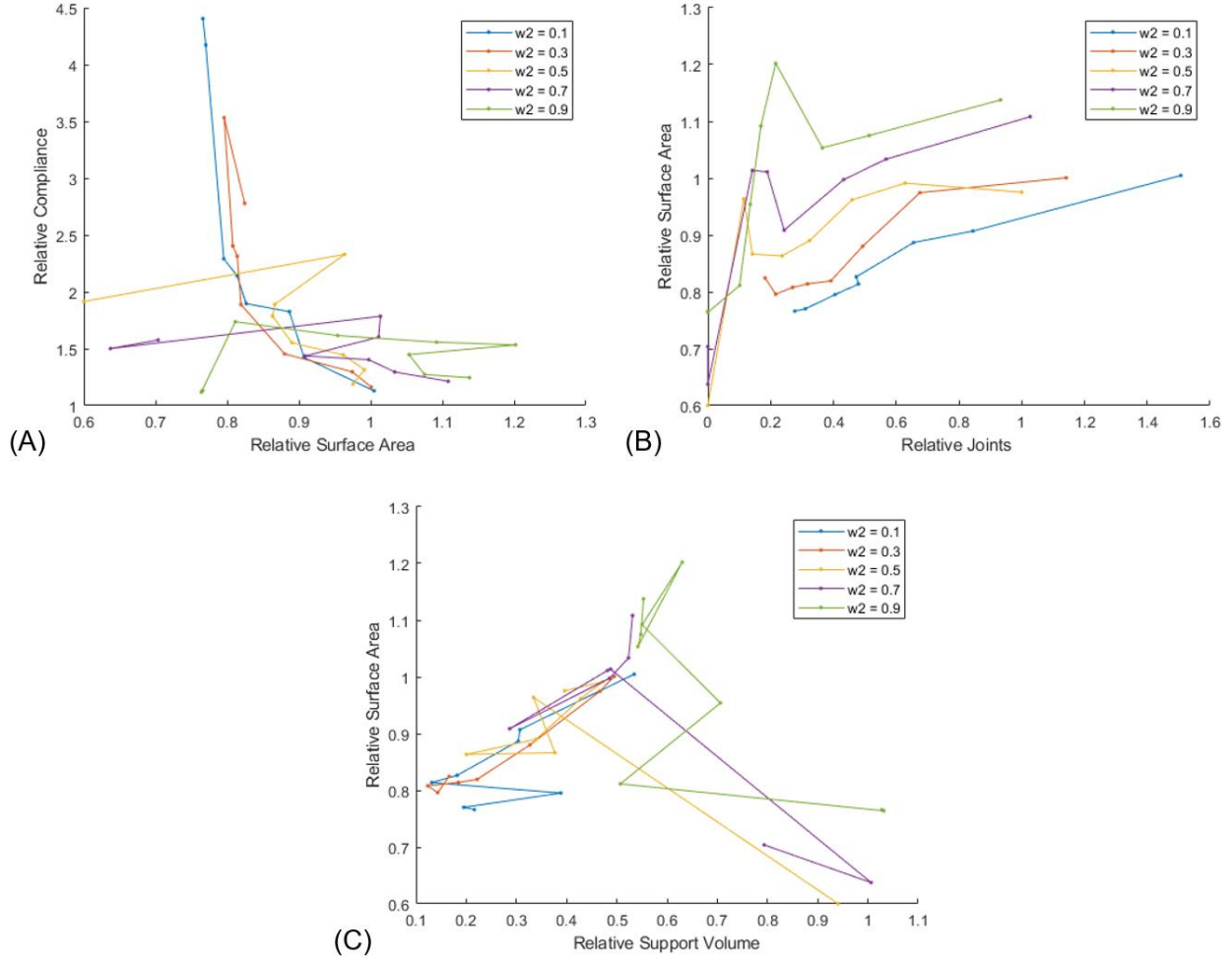


Figure 19: Parametric study results comparing surface area with other optimization objectives for MBB beam problem. All plots should be considered 2D side views of their respective 3D plots.

Pareto frontiers are generated from the optimization results to obtain a set of optimized design points for various trade-offs between two objectives. Figure 20 shows a Pareto curve comparing the relative support structure volume and relative number of joints in the assembly, all scaled using the baseline values as previously discussed. Optimized assembly designs are presented for select weightings showing the decrease in joints is again accompanied by a reduction in the number of parts in the assembly. Consolidating from four parts into a single part removed all joints from the design, but increased support structure volume from 12% to 79% of the baseline assembly. This indicates that there is indeed a trade-off occurring between AM costs and joint costs that should be considered during the part consolidation process. The specified ratio between AM printing costs and joining costs has a direct impact on the number of parts in the final assembly. As expected, lower w_2 values resulted in assembly designs with low support volume, while higher

w_2 values resulted in a single part design with larger support structure volume requirements.

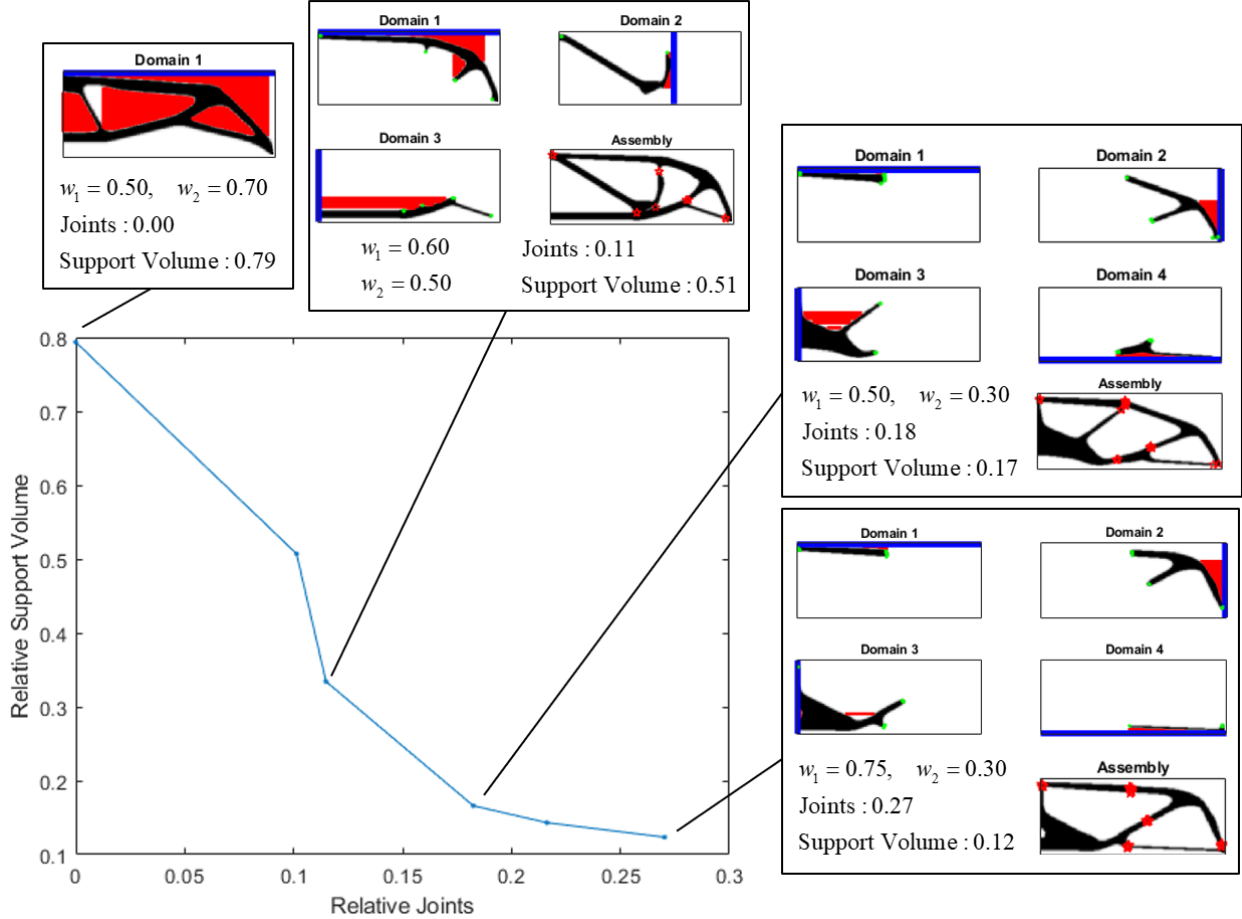


Figure 20: Pareto frontier of relative support structure volume compared to relative joints outlining the optimized designs from the MBB beam problem. Optimized designs along with their respective weighting factors are shown for select points.

A Pareto frontier of relative support volume and compliance in Figure 21 shows a similar trade-off between objectives with a decrease in support structure volume corresponding to an increase in compliance for the optimized designs. In this case, all optimized assemblies have four parts with varied topology and support structure volume requirements. The most significant design changes are apparent in domain 3, where the diagonal member originating from the upper left corner gradually shifts into a vertical member (relative to the build plate) and eventually merges with the other vertical member. This change in part design increases the structural compliance of the overall assembly, but significantly reduces the support volume requirements of the part in domain 3. Other changes are apparent in domain 2, where the member closest to the build plate at a 45-degree angle is pulled closer to the build plate thus decreasing support structure volume requirements. An 88% reduction in support structure volume was achieved with a 140% increase in compliance, however, it should be noted that the number of joints varies between designs.

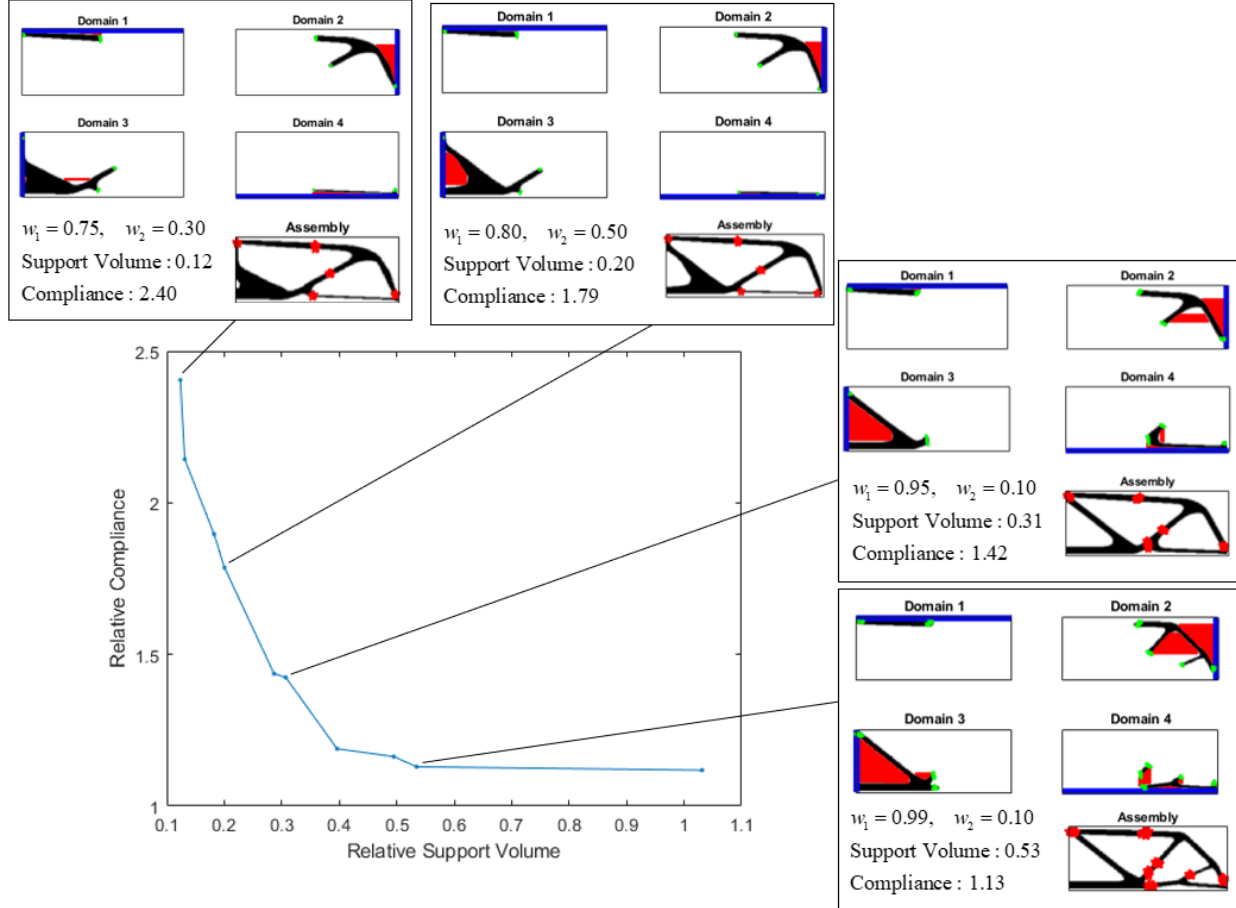


Figure 21: Pareto frontier of relative compliance compared to relative support structure volume for results from the MBB beam problem.

A meaningful Pareto frontier cannot be created between joints and compliance as there is a single optimal solution in terms of these objectives. Pareto frontiers were not investigated for surface area as the w_3 weighting was held constant. Finally, a Pareto surface was plotted in 3D space to illustrate the range of optimized solutions in terms of relative support structure volume, joints, and compliance. Figure 22 shows a plot of all optimized points along with an interpolated surface generated between the points using the MATLAB function *scatteredInterpolant.m*. A flat portion of the Pareto curve occurs where compliance is constant for varying trade-offs between support volume and number of joints. However, it is not possible to significantly reduce both support volume and joints without a corresponding increase in compliance. It can also be concluded that minimizing support structure volume has a larger influence on compliance when compared to minimizing joints.

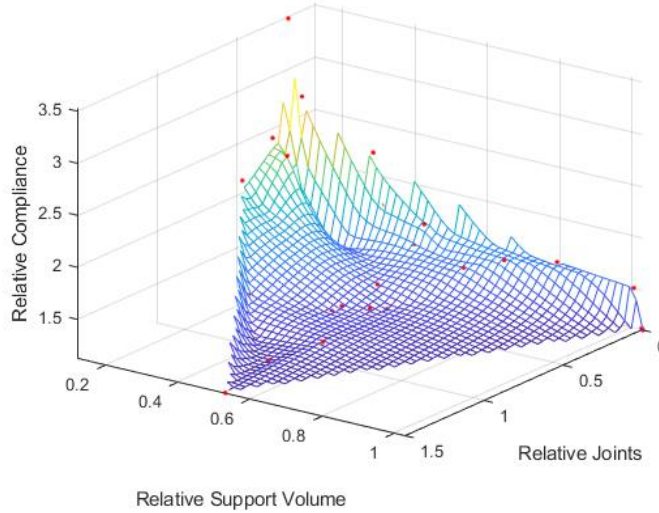


Figure 22: Pareto surface outlining the range of optimized solutions in terms of support volume, joints and compliance for an MBB beam problem. An interpolated surface is plotted between optimized results which are shown by red points.

3.2 Cantilever Beam (2D)

3.2.1 Joint Minimization

The 2D cantilever problem was optimized using a volume fraction of $\gamma = 0.3$ without considering AM cost factors using a weighting of $w_2 = 1$ over a range of structural-cost weightings between $w_1 = 0.2$ to $w_1 = 0.99$. The relative number of joints normalized with the largest objective result is summarized in Figure 23 along with the number of parts in each resultant design. This confirms the findings from the first problem that the MLTO technique can successfully consolidate assembly designs by varying the joint weighting factor and the initial joint density. The optimization resulted in a single part design when the structural-cost weighting was below a value of $w_1 = 0.6$, a similar range as seen in the MBB beam problem.

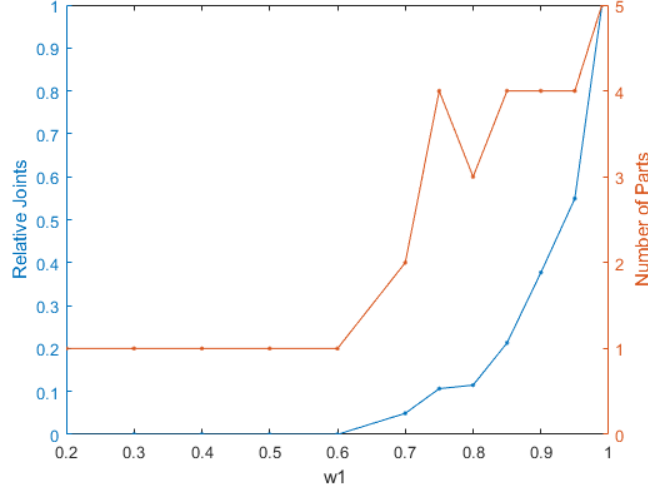


Figure 23: The number of parts and joints in the optimized assembly design for varying w_1 weightings of the 2D cantilever beam problem without considering AM part costs.

Assembly designs at four w_1 factors are displayed in Figure 24, outlining the decrease in number of parts as the structural-cost weighting is reduced with a constant weighting of $w_2 = 1$. The part consolidation from (A) to (B) and from (B) to (D) is accompanied by a decrease in compliance as the low-stiffness joints are removed from the assembly. The consolidation from (B) to (C) increases compliance due to convergence to a local minimum design. In this scenario, the MLTO optimization process could be repeated using only two part domains and new initial density gradients to avoid poor design convergence.

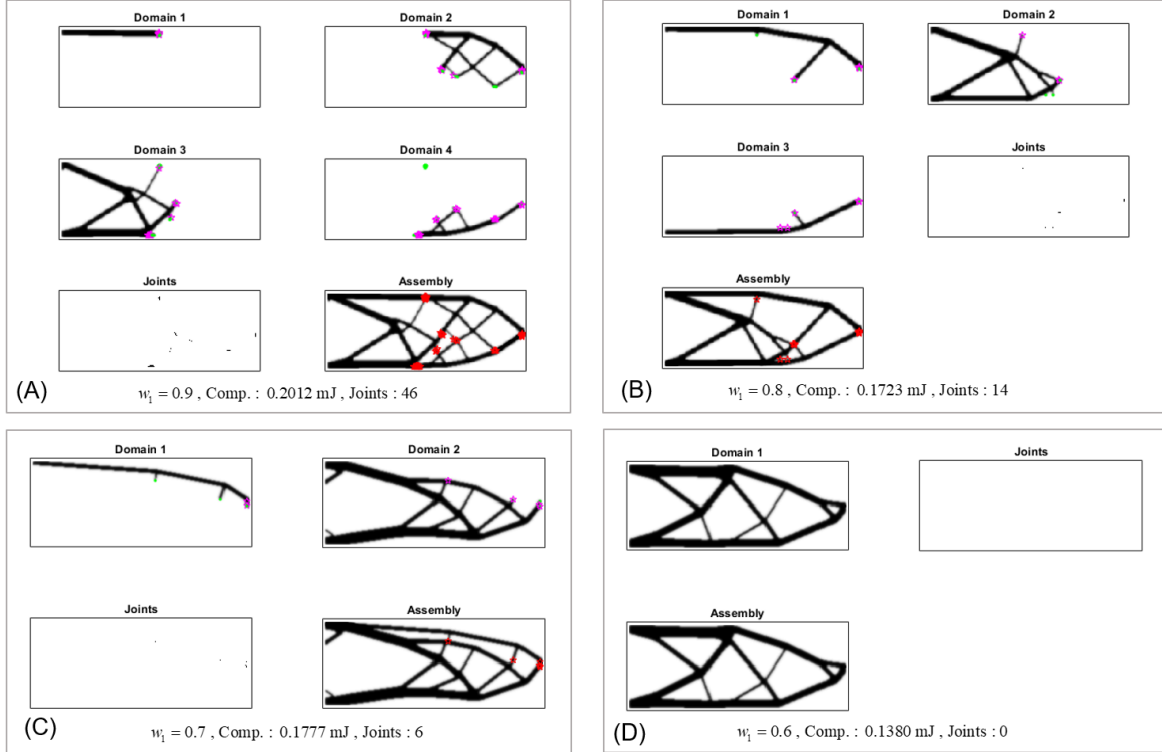


Figure 24: Optimized assembly designs for compliance and joint minimization of a 2D cantilever beam with varying structural-cost weightings.

3.2.2 Joint, Support Volume, and Surface Area Minimization

A parameter sweep was conducted for the simultaneous minimization of the number of joints, support volume, and surface area for the 2D cantilever beam problem with a volume fraction of $\gamma = 0.5$. The structural-cost weighting was again varied from $w_1 = 0.5$ to $w_1 = 0.99$ for values of $w_2 = 0.1, 0.3, 0.5, 0.7, 0.9$ and a fixed weighting of $w_3 = 0.9$. The maximum number of iterations was limited to 100 iterations per phase in this example. Figure 25 displays the optimization history results for the 2D cantilever beam problem with weightings focused on minimizing support structure volume. This example demonstrates a case where the algorithm converged to a four-part design by iteration 17, however the part in domain 1 is gradually removed between iterations 17-50. The optimization reached the maximum iteration limit for each phase because the high surface area weightings resulted in blurred exterior boundaries for each part, causing difficulties in convergence of the support structure volume objective. The design is sharpened after iteration 100 through the increase in penalty function and the final density thresholding.

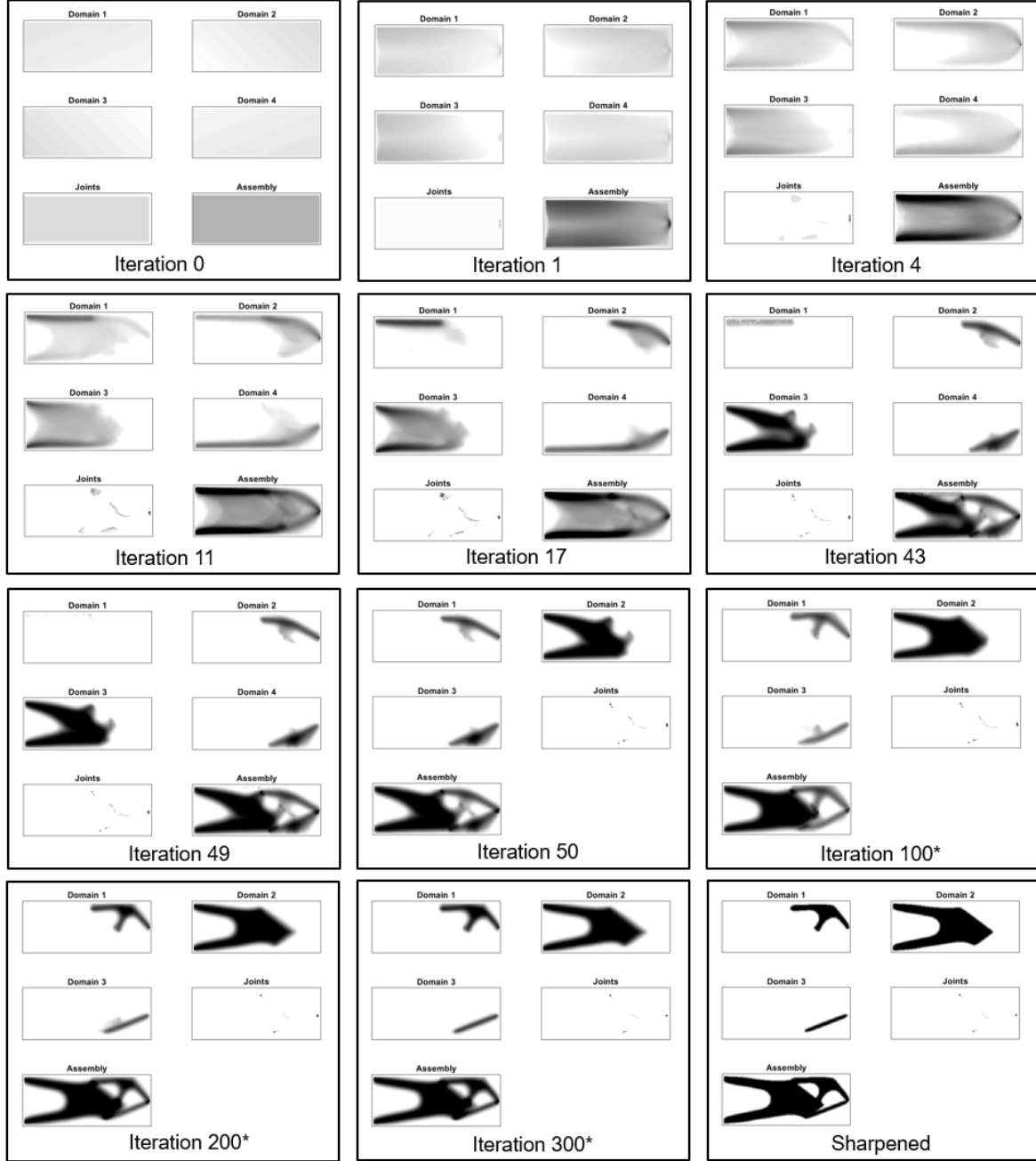


Figure 25: Optimization history of the 2D cantilever beam problem with a focus on support structure volume minimization ($w_1 = 0.50$, $w_2 = 0.30$)

Four optimized designs are summarized in Figure 26 where (A) presents the baseline single part design and (C) presents the baseline assembly design, both with minimal weightings applied to AM and joining cost factors. The objective values are measured relative to the baseline results to more easily compare between designs. The baseline assembly yields an 12% decrease in support volume with a 15% increase in compliance in addition to the added joint cost. The MLTO optimized design in Figure 26 (D) reduces support structure volume by 87% compared to the baseline single part using 8% of the joints compared to the baseline assembly. The reduction in

cost driving factors is associated with a 98% increase in structural compliance. The single part design from the MLTO algorithm in Figure 26 (B) reduces both support volume and surface area by about 44% with a 25% increase in compliance compared to the baseline single part result.

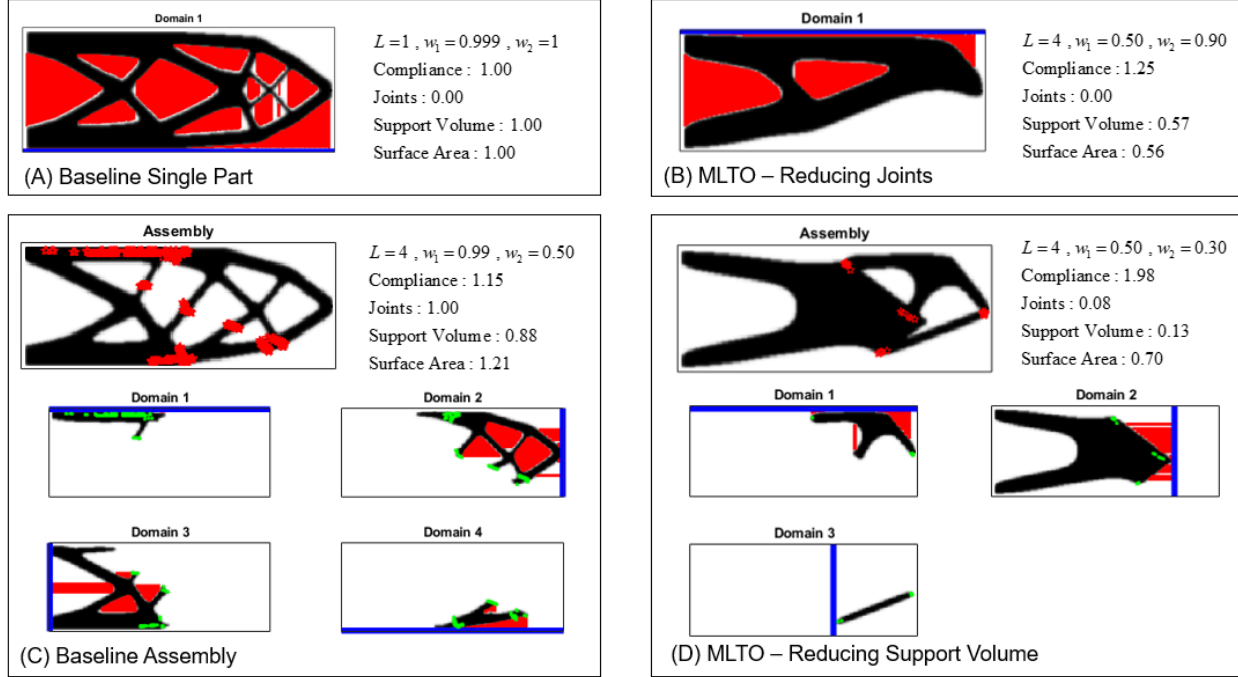


Figure 26: Summary of multi-objective optimization outlining the 2D cantilever beam results producing the lowest support structure volume and number of joints. (A) and (C) outline the baseline single part and assembly designs, while (B) and (D) outline the optimized designs with their respective cost weightings.

Figure 27 presents plots of objective function values across the parameter sweep measured relative to the baseline designs from Figure 26. The 3D plot in Figure 27 (A) outlines similar trends as the MBB beam problem with weightings above $w_2 = 0.5$ resulting in single part designs. In this case, the sweep along $w_2 = 0.5$ and $w_2 = 0.7$ resulted in a reduction in joints and support structure volume at the cost of significantly increased compliance. Meanwhile, the end result of the $w_2 = 0.9$ sweep reduced joints with relatively little change in both compliance and support structure volume (note there was a sharp increase in support structure volume with a near constant compliance, followed by a reduction in support structure volume associated with an increase in compliance). This confirms that it is not possible to significantly decrease all design objectives simultaneously and that a trade-off must be selected when consolidating an assembly.

The single part optimized designs resulted in a lower support structure volume than the baseline assembly (at the cost of increased compliance), causing the plot of support volume vs joints in Figure 27 (B) to demonstrate a decrease in both objectives. This indicates that a trade-off is not always apparent between these objectives if compliance is sacrificed as w_1 is lowered. The comparison of support structure volume and compliance in Figure 27 (C) indicates a general trend of increasing compliance as the support structure volume is reduced. Trends are less clear when following a fixed w_2 line, likely caused by convergence to different local minima as the number

of parts in the final assembly changes. Figure 27 (D) illustrates a clear increase in compliance as the number of joints is reduced for all w_2 weightings except for $w_2 = 0.9$. The increase in compliance is much less significant as w_2 increased.

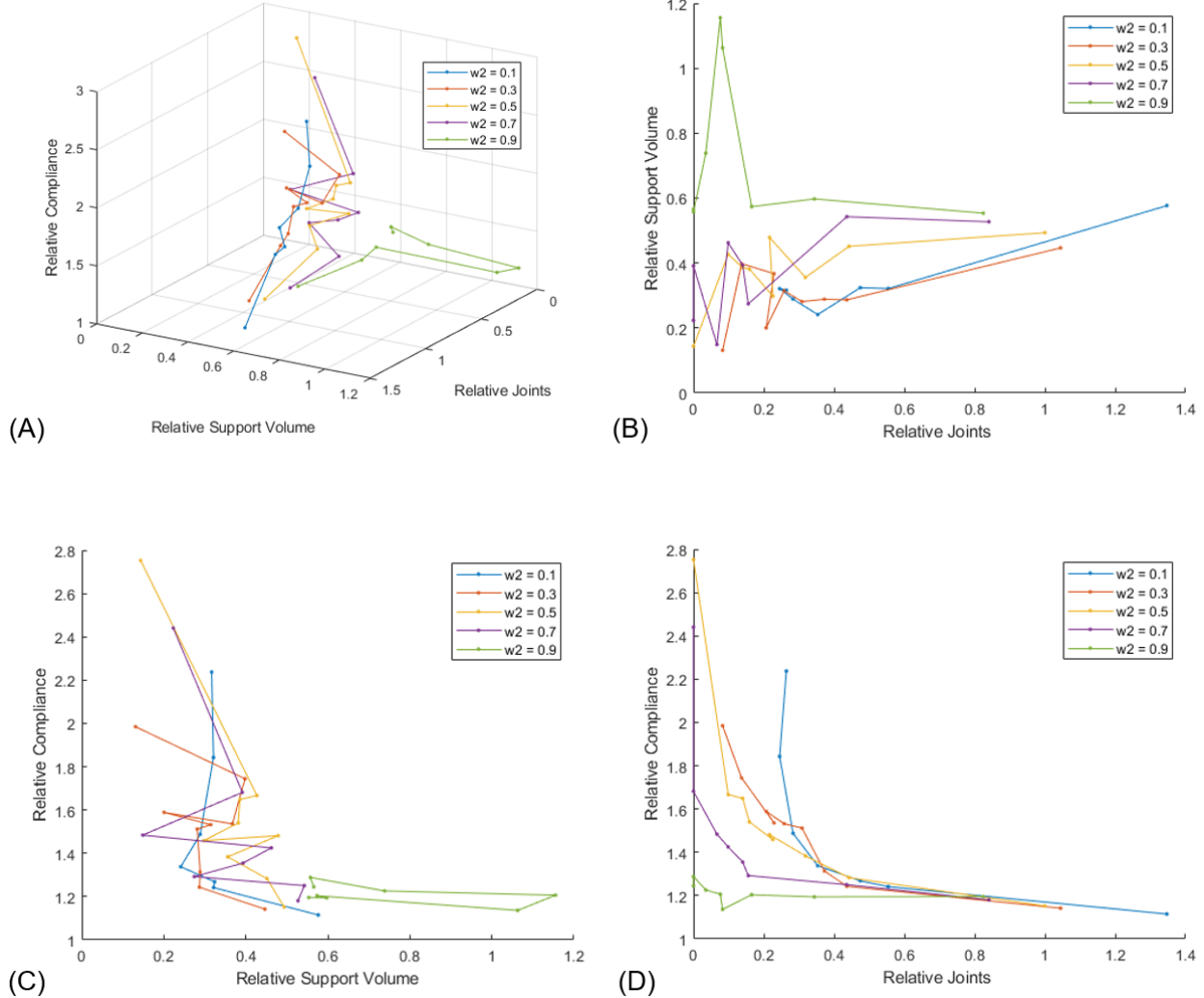


Figure 27: Visualization of parametric study results for minimization of relative support structure volume, joints, and compliance for the 2D cantilever beam test case with a 50% volume fraction. (A) plots the results for all weighting values in three dimensions indicate the trade-off of all objectives. (B)-(D) show 2D plane views of the results to analyze the performance of two objectives at a time.

Figure 27 (B) and (D) appear to indicate different overall trends from those seen in Figure 18 (B) and (D) despite the similarity in the trends in the 3D plots. This discrepancy is due to the fixed w_2 lines, which run along different paths of the 3D Pareto surface following different trade-offs between objectives and therefore indicate different trends when only focusing on two of the objectives. The relationship between all objectives should be considered in order to get a clear understanding of the implications of choosing weighting factors.

Figure 28 plots a Pareto curve of relative compliance and support structure volume taking only optimum points from the parameter study. A 42% reduction in support structure volume was achieved with a 12% increase in compliance. Further reduction in support volume resulted in a large increase in compliance ending in an 87% reduction in support volume with a 98% increase in compliance. There are significant differences in the geometry of the optimized designs indicating there are many local minima in the part consolidation problem. As the w_1 weighting decreases, the final assembly design deviates farther from the ideal cantilever structure as a result of reduced support structure volume.

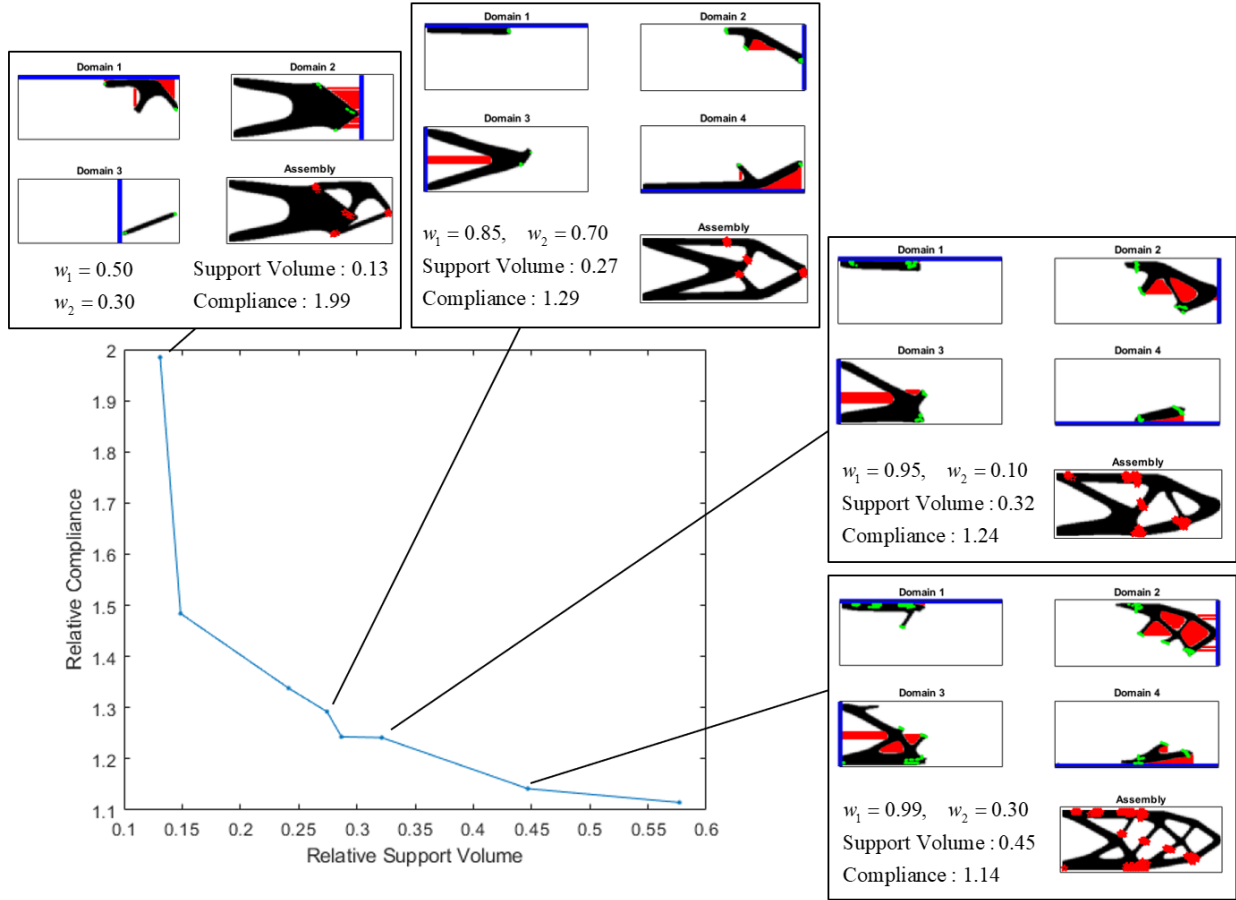


Figure 28: Pareto curve comparing relative compliance and support structure volume for the 2D cantilever beam problem with a 50% volume fraction. Final assembly designs are presented at select points.

The 3D Pareto surface interpolated between optimized design points in Figure 29 visually demonstrates the relationship between the relative compliance, joints, and support structure volume across the parameter sweep. It is evident that compliance and support structure are closely linked as any significant reduction in support structure volume was associated with a large increase in compliance. Joints and compliance are much less interdependent as it is possible to remove all joints without an increase in compliance. By understanding the relationship between these objectives, it is possible to select a desired trade-off for a specific use-case and generate an optimized design by assigning appropriate weighting factors.

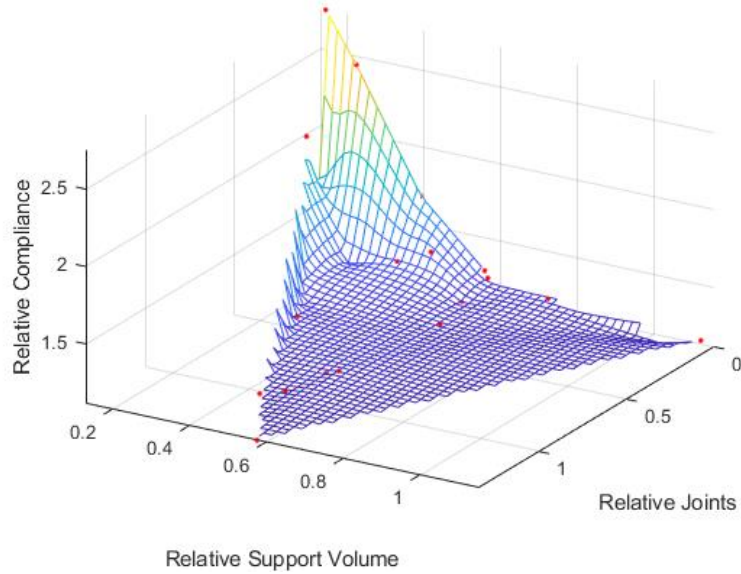


Figure 29: A Pareto surface outlining the relationship between relative support volume, joints, and compliance for the 2D cantilever beam problem with a volume fraction of 50%.

3.3 Cantilever Beam (3D)

3.2.1 Joint Minimization

The 3D cantilever beam problem was optimized for joint and compliance objectives using a weighting factor of $w_2 = 1$ and varying the structural-cost weighting between $w_1 = 0.2$ and $w_1 = 0.99$. A volume fraction of $\gamma = 0.3$ was used and two-part domains were initialized as per Figure 8. Optimized geometries and objective function values at select w_1 weighting factors are displayed in Figure 30. Results indicate that the approach effectively generated 3D cantilevered assembly structures with joints, shown in blue, existing only at the interfaces between parts. Without joint minimization in (A), the optimizer produces an assembly design with a large connection interface between parts. From (A) to (B), the increased weighting factor on joint minimization reduces the number of joints and produces a geometry with three distinct joining areas. The reduction in joining area between parts is accompanied by a 21% increase in compliance due to the decreased connection stiffness. With a weighting of $w_1 = 0.2$, the optimization converges to a single part design in (D) and achieves the lowest compliance solution.

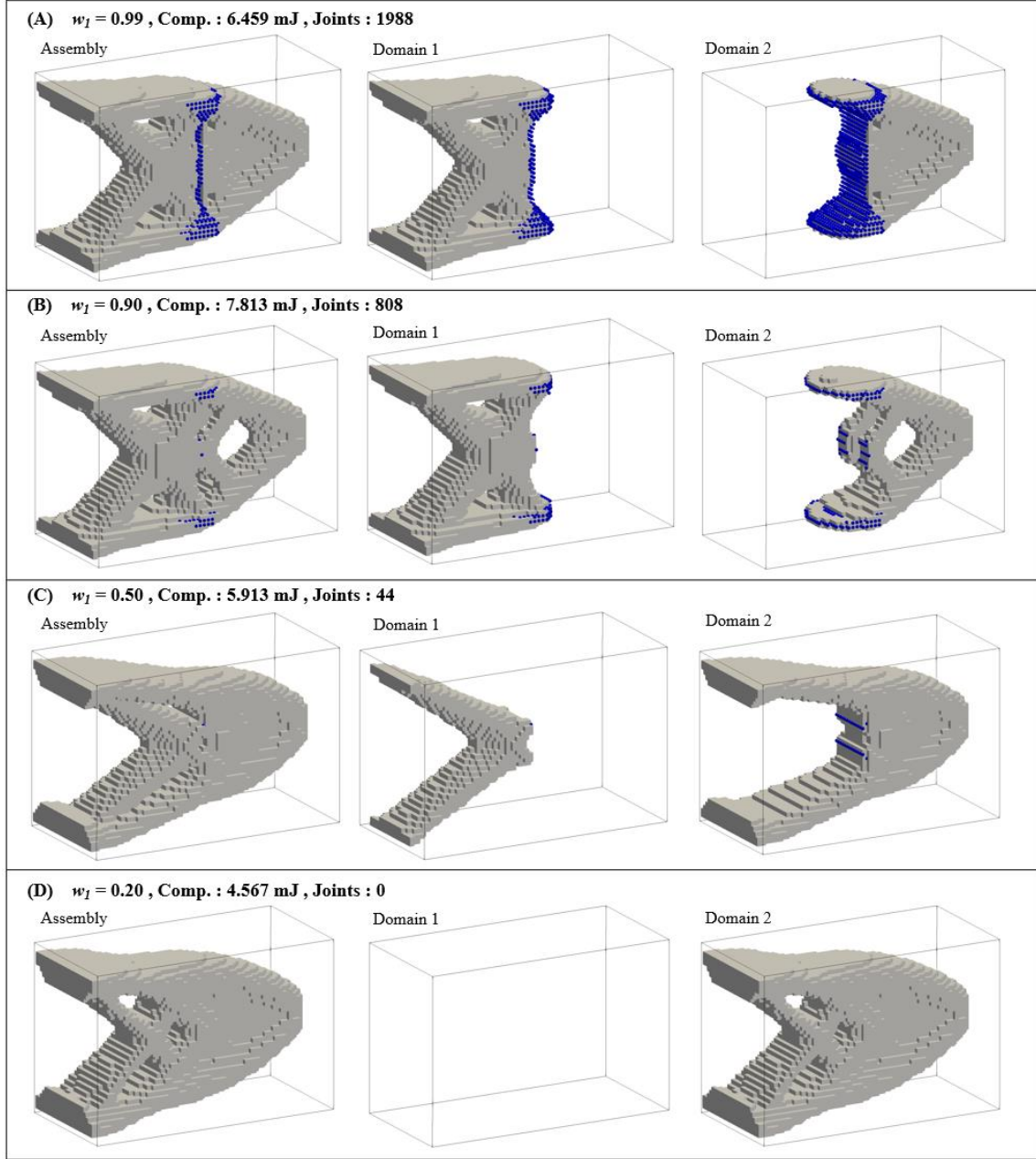


Figure 30: Optimized 3D cantilever beam assembly designs for compliance and joint minimization with various structural-cost weightings. Joints are depicted by blue points in assembly and part domains.

3.2.2 Joint, Support Volume, and Surface Area Minimization

The full problem statement was solved for the 3D cantilevered beam with a volume fraction of $\gamma = 0.3$ by using weighting factors of $w_2 = 0.1$ and $w_2 = 0.9$ to focus on minimizing AM costs or joining costs, respectively. The overall cost weighting was set to $w_1 = 0.8$ for a small cost weighting, and $w_1 = 0.2$ for a large weighting on cost. Figure 31 displays the optimized geometries in the assembly domain and the part domain, with support structure shown in red. The build direction of

each domain, shown by the red arrows, were selected a priori and were fixed throughout the optimization.

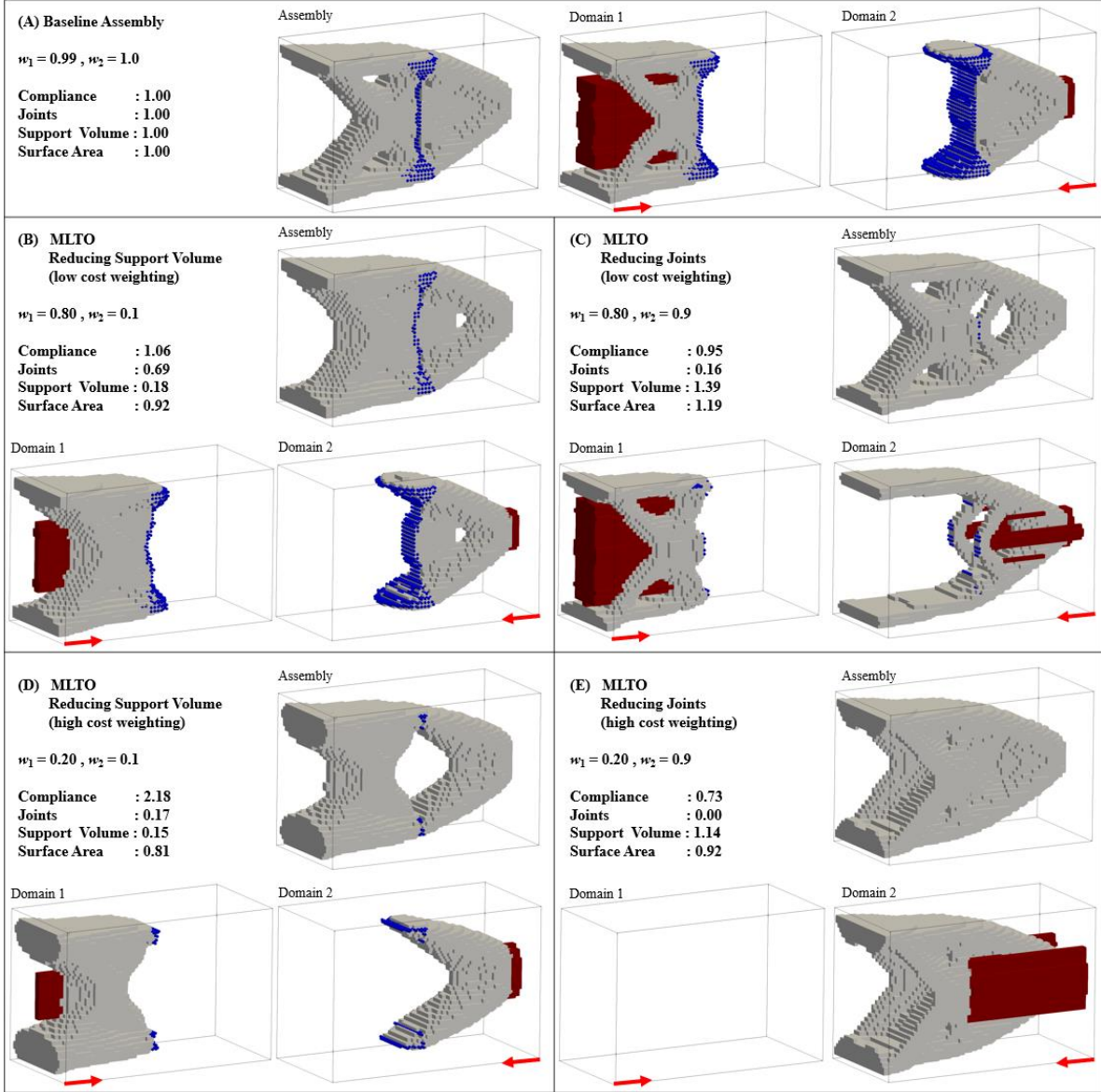


Figure 31: Optimized 3D cantilever beam assembly designs for MLTO of compliance, joint, and AM cost. Joints are depicted by blue points, support structure volume is depicted by red material, and the print direction of each domain is indicated by a red arrow.

Objective function values were normalized relative to the baseline design in Figure 31 (A), which had a large connection area and significant support structure requirements due to the overhanging geometry. When minimizing AM costs, the optimized design in (B) reduced support structure volume by 82% by changing the flat overhanging surface in Domain 1 to an angled surface that does not violate the self-supporting threshold. This reduction in support structure volume results in a 6% increase in compliance. When further increasing the overall cost weighting in (D), both AM and joining costs were significantly reduced, however compliance was increased by 118%.

Shown in (C), a small cost weighting focused on minimizing joints yielded an 84% reduction in joints but increased support volume and surface area, highlighting the trade-off between AM costs and joining costs. The fully consolidated design in (E) had a 23% reduction in compliance but a 14% increase in support structure volume, as multiple build orientations were no longer used in different parts of the geometry.

5 CONCLUSIONS

This work presented a novel methodology capable of determining the optimal number of parts, part geometry, and connection layout for an additive manufacturing assembly design. The MLTO approach was formulated to setup and perform assembly-level topology optimization in a bottom-up approach that eliminates any bias towards the original assembly design that is prevalent in other part consolidation research. Additive manufacturing cost driving factors are calculated and joining costs are represented by the total number of joints in the assembly. The multi-objective optimization problem statement uses a gradient-based optimizer to minimize the weighted sum of compliance, support structure volume, surface area, and number of joints in order to consider the total cost of the assembly. By considering the complex mechanisms relating these objectives, the MLTO approach can generate consolidated designs based on the desired trade-offs between structural performance, joint cost, and print cost.

The part consolidation methodology was demonstrated using three numerical examples which indicated that the algorithm can generate either a single part design or a multi-part assembly with an ideal connection layout based on the selection of weighting factors. A sweep of multi-objective weighting factors was conducted to study the relationship between design objectives. Pareto curves and surfaces generated a set of optimized designs with varied objective trade-offs. Results indicate that a reduction in support structure volume is associated with a significant increase in structural compliance, which is consistent with previous studies [11-13]. The number of joints in an assembly can be reduced without a corresponding increase in compliance only if the number of parts in the assembly also decreases. Both joint and AM cost factors cannot be simultaneously minimized without sacrificing the structural performance of the final design.

The boundary condition placement and design variable initialization discussed in this work remove bias towards initial assembly design by starting with a clean slate approach. However, the resultant assembly design is influenced by the selection of the initial density gradient distribution. This effect was reduced through careful selection of initial parameters, however additional investigation into alternative problem initialization approaches and other optimization parameters should be conducted in future work to improve optimization convergence and the quality of the optimized solutions. The selection of build orientation is critical for the reduction in support structure volume, and the manual identification of the ideal printing angle is more challenging when multiple parts are introduced. Therefore, the implementation of an automatic selection of build orientation for each part is an important addition to any part consolidation algorithm. The build height of a part affects printing cost and time and should be considered when selecting the ideal part orientation. Future extension to consider 3D complex geometry is essential to solving real-world part consolidation problems. Some of the presented results contain parts with significant overlaps in

geometry, which must be addressed when solving 3D problems in order to have a physically meaningful design. Finally, additional AM factors should be integrated with the approach, such as print bed size constraints and the removal of internal voids.

DATA AVAILABILITY STATEMENT

The data that support the findings of this study are available from the corresponding author upon reasonable request.

REFERENCES

1. Gu DD, Meiners W, Wissenbach K, Poprawe R. Laser additive manufacturing of metallic components: materials, processes and mechanisms. *Int Mater Rev.* 2012;57(3):133-164. doi:10.1179/1743280411y.0000000014
2. Frazier WE. Metal Additive Manufacturing: A Review. *J Mater Eng Perform.* 2014;23(6):1917-1928. doi:10.1007/s11665-014-0958-z
3. Bendsoe MP, Kikuchi N. Generating Optimal Topologies in Structural Design Using a Homogenization Method. *Comput Meth Appl Mech Eng.* 1988;71(2):197-224. doi:10.1016/0045-7825(88)90086-2
4. Deaton JD, Grandhi RV. A survey of structural and multidisciplinary continuum topology optimization: post 2000. *Struct Multidiscip Optim.* 2014;49(1):1-38. doi:10.1007/s00158-013-0956-z
5. Sigmund O, Maute K. Topology optimization approaches A comparative review. *Struct Multidiscip Optim.* 2013;48(6):1031-1055. doi:10.1007/s00158-013-0978-6
6. Wong J, Ryan L, Kim IY. Design optimization of aircraft landing gear assembly under dynamic loading. *Struct Multidiscip Optim.* 2018;57(3):1357-1375. doi:10.1007/s00158-017-1817-y
7. Li C, Kim IY, Jeswiet J. Conceptual and detailed design of an automotive engine cradle by using topology, shape, and size optimization. *Struct Multidiscip Optim.* 2015;51(2):547-564. doi:10.1007/s00158-014-1151-6
8. Guirguis D, Aulig N, Picelli R, et al. Evolutionary Black-Box Topology Optimization: Challenges and Promises. *IEEE Trans. Evol. Comput.* 2020;24(4):613-633. doi:10.1109/tevc.2019.2954411
9. Thompson MK, Moroni G, Vaneker T, et al. Design for Additive Manufacturing: Trends, opportunities, considerations, and constraints. *Cirp Ann-Manuf Techn.* 2016;65(2):737-760. doi:10.1016/j.cirp.2016.05.004
10. Liu JK, Gaynor AT, Chen SK, et al. Current and future trends in topology optimization for additive manufacturing. *Struct Multidiscip Optim.* 2018;57(6):2457-2483. doi:10.1007/s00158-018-1994-3
11. Mhapsekar K, McConaha M, Anand S. Additive Manufacturing Constraints in Topology Optimization for Improved Manufacturability. *J Manuf Sci E-T Asme.* 2018;140(5). doi:10.1115/1.4039198
12. Langelaar M. Combined optimization of part topology, support structure layout and build orientation for additive manufacturing. *Struct Multidiscip Optim.* 2018;57(5):1985-2004. doi:10.1007/s00158-017-1877-z

13. Ryan L, Kim IY. A multiobjective topology optimization approach for cost and time minimization in additive manufacturing. *Int J Numer Methods Eng.* 2019;118(7):371-394. doi:10.1002/nme.6017
14. Sabiston G, Kim IY. 3D topology optimization for cost and time minimization in additive manufacturing. *Struct Multidiscip Optim.* 2019;61:731-748. doi:10.1007/s00158-019-02392-7
15. Mezzadri F, Bouriakov V, Qian XP. Topology optimization of self-supporting support structures for additive manufacturing. *Addit. Manuf.* 2018;21:666-682. doi:10.1016/j.addma.2018.04.016
16. Schmitt M, Mehta RM, Kim IY. Additive manufacturing infill optimization for automotive 3D-printed ABS components. *Rapid Prototyp J.* 2019. doi:10.1108/RPJ-01-2019-0007
17. Stevenson A, Baumers M, Segal J, Macdonell S. How Significant Is the Cost Impact of Part Consolidation. In: Proceedings of the Solid Freeform Fabrication Symposium; 2017; Austin, TX.
18. Schmelzle J, Kline EV, Dickman CJ, Reutzel EW, Jones G, Simpson TW. (Re)Designing for Part Consolidation: Understanding the Challenges of Metal Additive Manufacturing. *J Mech Design.* 2015;137(11). doi:10.1115/1.4031156
19. Yang S, Zhao YF. Additive Manufacturing-Enabled Part Count Reduction: A Lifecycle Perspective. *J Mech Design.* 2018;140(3). doi:10.1115/1.4038922
20. Knofius N, van der Heijden MC, Zijm WHM. Consolidating spare parts for asset maintenance with additive manufacturing. *Int J Prod Econ.* 2019;208:269-280. doi:10.1016/j.ijpe.2018.11.007
21. Oh Y, Zhou C, Behdad S. Part decomposition and assembly-based (Re) design for additive manufacturing: A review. *Addit. Manuf.* 2018;22:230-242. doi:10.1016/j.addma.2018.04.018
22. Oh Y, Behdad S, Zhou C. Part Separation Methods for Assembly Based Design in Additive Manufacturing. In: Proceedings of the International Design Engineering Technical Conferences and Computers and Information in Engineering Conference; 2017; Cleveland, OH. doi:10.1115/DETC2017-68002
23. Guirguis D, Hamza K, Aly M, Hegazi H, Saitou K. Multi-objective topology optimization of multi-component continuum structures via a Kriging-interpolated level set approach. *Struct. Multidiscip. Optim.* 2015;51(3):733-748. doi:10.1007/s00158-014-1154-3
24. Guirguis D, Melek WW, Aly MF. High-resolution non-gradient topology optimization. *J. Comput. Phys.* 2018;372:107-125. doi:10.1016/j.jcp.2018.06.025
25. Liu JK. Guidelines for AM part consolidation. *Virtual Phys Prototy.* 2016;11(2):133-141. doi:10.1080/17452759.2016.1175154
26. Rodrigue H, Rivette M. An assembly-level design for additive manufacturing methodology. In: Proceedings of the IDMME-Virtual Concept; 2010; France.
27. Yang S, Tang YL, Zhao YF. A new part consolidation method to embrace the design freedom of additive manufacturing. *J Manuf Process.* 2015;20:444-449. doi:10.1016/j.jmapro.2015.06.024
28. Sossou G, Demoly F, Montavon G, Gomes S. An additive manufacturing oriented design approach to mechanical assemblies. *J Comput Des Eng.* 2018;5(1):3-18. doi:10.1016/j.jcde.2017.11.005

29. Reiher T, Lindemann C, Jahnke U, Deppe G, Koch R. Holistic approach for industrializing AM technology: from part selection to test and verification. *Prog Addit Manuf.* 2017;2(1):43-55. doi:10.1007/s40964-017-0018-y
30. Yang S, Santoro F, Zhao YF. Towards a Numerical Approach of Finding Candidates for Additive Manufacturing-Enabled Part Consolidation. *J Mech Design.* 2018;140(4). doi:10.1115/1.4038923
31. Chickermane H, Gea HC. Design of multi-component structural systems for optimal layout topology and joint locations. *Eng Comput.* 1997;13(4):235-243. doi:10.1007/Bf01200050
32. Li Q, Steven GP, Xie YM. Evolutionary structural optimization for connection topology design of multi-component systems. *Eng Computation.* 2001;18(3-4):460-479. doi:10.1108/02644400110387127
33. Zhu JH, Gao HH, Zhang WH, Zhou Y. A Multi-point constraints based integrated layout and topology optimization design of multi-component systems. *Struct Multidiscip Optim.* 2015;51(2):397-407. doi:10.1007/s00158-014-1134-7
34. Swartz KE, James KA. Gaussian Layer Connectivity Parameterization: A New Approach to Topology Optimization of Multi-Body Mechanisms. *Comput.-Aided Des.* 2019;115:42-51. doi:10.1016/j.cad.2019.05.008
35. Zhou Y, Nomura T, Saitou K. Multicomponent Topology Optimization for Additive Manufacturing With Build Volume and Cavity Free Constraints. *J Comput Inf Sci Eng.* 2019;19(2). doi:10.1115/1.4042640
36. Zhou Y, Nomura T, Saitou K. Multi-component topology and material orientation design of composite structures (MTO-C). *Comput Meth Appl Mech Eng.* 2018;342:438-457. doi:10.1016/j.cma.2018.07.039
37. Crispo L, Kim IY. Assembly Level Topology Optimization Towards a Part Consolidation Algorithm for Additive Manufacturing. In: AIAA SciTech 2020 Forum; 2020; Florida, USA. doi:10.2514/6.2020-0893
38. Li D, Kim IY. Multi-material topology optimization for practical lightweight design. *Struct Multidiscip Optim.* 2018;58(3):1081-1094. doi:10.1007/s00158-018-1953-z
39. Woischwill C, Kim IY. Multimaterial multijoint topology optimization. *Int J Numer Methods Eng.* 2018;115(13):1552-1579. doi:10.1002/nme.5908
40. Florea V, Pamwar M, Sangha B, Kim IY. 3D multi-material and multi-joint topology optimization with tooling accessibility constraints. *Struct Multidiscip Optim.* 2019. doi:10.1007/s00158-019-02344-1
41. Sigmund O. Morphology-based black and white filters for topology optimization. *Struct Multidiscip Optim.* 2007;33:401-424. doi:10.1007/s00158-006-0087-x
42. Chandregowda S, Reddy GRC. Evaluation of Fastener Stiffness Modelling Methods for Aircraft Structural Joints. In: Advances in Mechanical Design, Materials and Manufacture; 2018; India. doi:10.1063/1.5029577
43. Kawamoto A, Matsumori T, Yamasaki S, Nomura T, Kondoh T, Nishiwaki S. Heaviside projection based topology optimization by a PDE-filtered scalar function. *Struct Multidiscip Optim.* 2011;44(1):19-24. doi:10.1007/s00158-010-0562-2
44. Lazarov BS, Sigmund O. Filters in topology optimization based on Helmholtz-type differential equations. *Int J Numer Methods Eng.* 2011;86(6):765-781. doi:10.1002/nme.3072

45. Sigmund O, Petersson J. Numerical instabilities in topology optimization: A survey on procedures dealing with checkerboards, mesh-dependencies and local minima. *Struct Optim.* 1998;16(1):68-75. doi:10.1007/Bf01214002
46. Zhou M, Shyy YK, Thomas HL. Checkerboard and minimum member size control in topology optimization. *Struct Multidiscip Optim.* 2001;21(2):152-158. doi:10.1007/s001580050179
47. Qian XP. Undercut and overhang angle control in topology optimization: A density gradient based integral approach. *Int J Numer Methods Eng.* 2017;111(3):247-272. doi:10.1002/nme.5461
48. Clausen A, Andreassen E. On filter boundary conditions in topology optimization. *Struct Multidiscip Optim.* 2017;56(5):1147-1155. doi:10.1007/s00158-017-1709-1
49. Svanberg K. The Method of Moving Asymptotes - a New Method for Structural Optimization. *Int. J. Numer. Methods Eng.* 1987;24(2):359-373. doi:10.1002/nme.1620240207
50. Wang FW, Lazarov BS, Sigmund O. On projection methods, convergence and robust formulations in topology optimization. *Struct. Multidiscip. Optim.* 2011;43(6):767-784. doi:10.1007/s00158-010-0602-y

Appendix A

Verification of the analytical sensitivities was conducted using finite differencing method (FDM) on an 80 x 40 element MBB beam using 2 part domain layers. Compliance sensitivity verification (with respect to element and joint density) has been included below. Interested readers are referred to Ryan and Kim [13] for detailed verification of the surface area and support structure volume sensitivity analysis used in this work. Verification of the joint cost sensitivity is trivial as the sensitivities are equal to unity ($d\Gamma / dy_j = 1$). The optimization was stopped after 6 iterations to obtain intermediate topology results shown in Figure A1 below. Sampling locations were selected at random for all domains and are indicated by solid black squares in the part and joining domains. FDM sensitivities were calculated with a step size of $\Delta x_e = 0.001$ using the forward difference method.

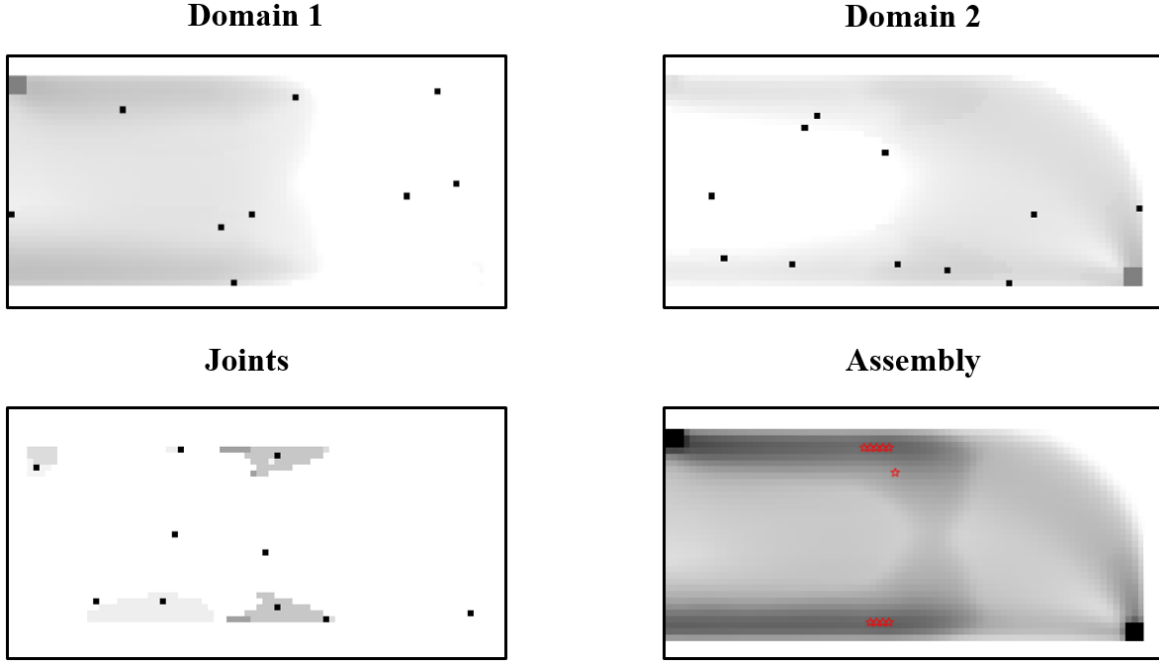


Figure A1: Intermediate topology results used for FDM sensitivity verification. Solid black squares indicate the elements randomly selected for the verification process.

Table A1 and A2 outline the results of the FDM sensitivity verification, showing excellent agreement between all analytical and FDM sensitivities. Note that design variables with near zero values have sensitivities that are effectively zero, and the verification column is not computed for these elements.

Table A1: FDM verification of compliance sensitivity analysis with respect to element density.

Element Design Variable (x_e)	FDM ($\Delta C / \Delta x_e \times 10^3$)	Analytical ($\partial C / \partial x_e \times 10^3$)	Verification ($\frac{\Delta C / \Delta x_e}{\partial C / \partial x_e} \times 100\%$)
2583	0.0000	0.0000	-
5437	-2.4513	-2.4522	99.96%
3503	0.0000	0.0000	-
2766	0.0000	0.0000	-
729	-3.3916	-3.3926	99.97%
26	-0.7860	-0.7866	99.92%
4034	-0.9655	-0.9663	99.92%
3593	-0.5315	-0.5320	99.91%
5586	-3.0051	-3.0066	99.95%
2901	0.0000	0.0000	-
1388	-2.3996	-2.4007	99.96%
5035	-4.4984	-4.5004	99.96%
6265	-1.3307	-1.3311	99.97%

4714	-3.8836	-3.8850	99.96%
1586	-2.2576	-2.2589	99.95%
1477	-2.9601	-2.9611	99.97%
4092	-0.0231	-0.0231	100.01%
4616	-0.0596	-0.0595	100.16%
4170	-0.2875	-0.2877	99.93%
1847	-2.0812	-2.0822	99.95%

Table A2: FDM verification of compliance sensitivity analysis with respect to joint density.

Joint Design Variable (y_i)	FDM ($\Delta C / \Delta y_i \times 10^3$)	Analytical ($\partial C / \partial y_i \times 10^3$)	Verification ($\frac{\Delta C / \Delta y_i}{\partial C / \partial y_i} \times 100\%$)
1149	0.0000	0.0000	-
664	-0.3111	-0.3091	100.65%
726	-0.2317	-0.2301	100.71%
1216	-1.9411	-1.9378	100.17%
711	0.0000	0.0000	-
33	-0.0016	-0.0016	100.92%
1191	-2.0808	-2.0772	100.17%
2145	0.0000	0.0000	-
1450	-0.8959	-0.8969	99.89%
345	0.0000	0.0000	-